

CHARACTERIZATION OF STRESS-INDUCED CRACKS IN ROCKS

by

MICHAEL L. FEVES

B.A., Reed College  
(1973)

SUBMITTED IN PARTIAL FULFILLMENT  
OF THE REQUIREMENTS FOR THE  
DEGREE OF

DOCTOR OF PHILOSOPHY

at the

MASSACHUSETTS INSTITUTE OF TECHNOLOGY  
(August, 1977)

Signature of Author.....  
Department of Earth and Planetary Sciences  
August 12, 1977

Certified by.....  
Thesis Supervisor

Accepted by.....  
Chairman, Departmental Committee on Graduate Students

~~Under~~  
**WITHDRAWN**  
**FROM**  
DEC 30 1977  
**MIT LIBRARIES**

## CHARACTERIZATION OF STRESS-INDUCED CRACKS IN ROCKS

by

MICHAEL L. FEVES

Submitted to the Department of Earth and Planetary Sciences  
on August 12, 1977 in partial fulfillment of the requirements  
for the Degree of Doctor of Philosophy

## ABSTRACT

Cracks produced in several samples of crustal igneous rocks by uniaxial stress have been examined with the scanning electron microscope, the petrographic microscope, and by measurements of strain to high precision as a function of hydrostatic pressure. Our data on laboratory stressed rocks show that stress-induced crack porosity is directly related to initial crack porosity and failure strength is inversely related to pre-existing crack porosity. Stress-induced cracks (SIC): (1) are intragranular or transgranular, (2) are typically planar, (3) may cross several grain boundaries, (4) form parallel to subparallel sets, (5) may be associated with partially healed cracks, and (6) close at hydrostatic pressures of 100 to 200 bars. Cracks with all of these characteristics are found in a granite core from Shannon County, Missouri. SIC in the Shannon County core are only present below 1 km and are oriented in a vertical plane. Through analysis of SIC in this core we have determined that the magnitude of the maximum compressive stress is greater than the tensile strength of the granite (~100 bars) and is directed horizontally.

The effects of cycling rocks with hydrostatic pressure and also with uniaxial loading have been examined. Uniaxial stress cycling increases total crack porosity in Westerly (RI) granite after each cycle, but no increase in crack porosity is observed in repeatedly stressed Frederick (MD) diabase. We attribute this behavior to the fact that pre-existing cracks enhance the production of SIC. Unstressed Westerly granite contains many cracks but Frederick diabase is virtually crack-free. Hydrostatic pressure cycling reduces total crack porosity by 20 to 50 percent between the first and second cycles, but less than 30 percent between the second and third cycles.

These data indicate that many cracks do not reopen completely when the pressure is removed. Therefore, laboratory experiments done under simulated in situ conditions of pressure and temperature may not be valid analogues.

Name and Title of Thesis Supervisor: Gene Simmons  
Professor of Geophysics

## ACKNOWLEDGEMENTS

My wife, Gloria, and my daughter, Jordana, gave me the 'inspiration' to complete my thesis. They often bore the brunt of my frustrations when experimental problems developed, and they spent many evenings and weekends alone, while I was at the lab (drinking beer). I thank them for their steadfast support.

I am particularly indebted to my advisor, Gene Simmons, who constantly supplied constructive criticism and new ideas in all aspects of my work. He was never too busy to stop what he was doing and discuss results or 'show me the light' when something went wrong.

I have benefited from discussions with many people during my internment at MIT. Michael Batzle, Bill Brace, Herman Cooper, Mike Fehler, Frank Miller, Elaine Padovani, Dorothy Richter, Steve Shirey, and Bob Siegfried were eager to offer suggestions and criticism (constructive and otherwise). Prior to recent automation of the DSA equipment, collection of DSA data required hundreds of hours of continuous operator attention. Michael Batzle, Herman Cooper, Mike Fehler, Ann Harlow, and Bob Siegfried spent many nearly sleepless nights taking DSA data (and drinking beer). Bob Siegfried developed the computer programs used to analyze the DSA data and Frank Miller designed and maintained the electronics associated with the DSA and acoustic emission systems. Bill Brace provided the pressure equipment used to stress most of the samples.

Financial support was provided by Office of Naval  
Research contract N00014-76-C-0478.

## TABLE OF CONTENTS

	Page
Abstract	2
Acknowledgements	4
List of Figures	7
List of Tables	9
Chapter 1: Introduction	10
Chapter 2: Experimental Considerations	14
Chapter 3: Characterization of Laboratory Stress- Induced Cracks	34
Chapter 4: Effects of Hydrostatic Pressure Cycling and Uniaxial Stress Cycling	64
Chapter 5: Analysis of SIC in a Granite Core	81
Chapter 6: Summary	101
References	110
Biographical Note	123

## LIST OF FIGURES

	Page
2.1 Sample location map.	15
2.2 Block diagram of acoustic emission and stress monitoring system.	24
2.3 Acoustic emission rate and stress versus time.	27
2.4 Components of DSA compression curve.	30
3.1 Microcracks in unstressed Wausau (WI) granite.	37
3.2 Growth of crystals in fluid inclusion.	38
3.3 Typical texture of unstressed Westerly (RI) granite.	39
3.4 Partially healed crack in quartz.	40
3.5 Typical texture of unstressed Graniteville (MO) granite.	41
3.6 Typical texture of stressed Graniteville (MO) granite.	43
3.7 SIC associated with pre-existing cracks in Graniteville (MO) granite.	45
3.8 Stress-induced elongation of pre-existing crack in quartz.	46
3.9 Crack closure pressure spectra for unstressed and stressed Westerly (RI) granite.	49
3.10 Crack closure pressure spectra for unstressed and stressed Graniteville (MO) granite.	50
3.11 Crack closure pressure spectra for unstressed and stressed Mt. Airy (NC) granite.	51

	-Page
3.12 Empirical relationship between initial crack porosity and stress-induced crack porosity.	52
3.13 Empirical relationship between failure strength and initial crack porosity.	56
3.14 Relationship between seismic ray paths and crack orientation.	62
4.1 Crack closure pressure spectra for restressed Westerly (RI) granite.	71
5.1 Location map for Sh-13 core.	84
5.2 Crack porosity versus depth in southeastern Missouri.	86
5.3 Crack closure pressure spectra for various depths in Sh-13.	89
5.4 Orientation of SIC in Sh-13.	90
5.5 Typical texture of Sh-13-1523.	93
5.6 Transgranular stress-induced crack in Sh-13-1056.	94
5.7 Typical texture of samples from above 1 km in Sh-13.	95
5.8 Fracturing episodes in Sh-13.	97



## LIST OF TABLES

	Page
2.1 Modal Analysis	16
2.2 Sample Descriptions	18
2.3 Maximum Uniaxial Stress	25
3.1 List of Abbreviations	36
3.2 Change in Crack Porosity due to Stressing	53
3.3 Mean Strength and Initial Crack Porosity	57
4.1 Changes in $\zeta(P)$ due to Hydrostatic Pressure Cycling	66
4.2 $\zeta(2kb)$ for Stress-Cycled Westerly Granite	73
4.3 $\zeta(2kb)$ for Stress-Cycled Frederick Diabase	74
5.1 Modal Analysis of Sh-13 as a Function of Depth	82
5.2 Crack Porosity as a Function of Depth for Sh-13	87

CHAPTER 1  
INTRODUCTION

Mechanical properties of rocks under stress have been studied extensively (Brace, 1964, 1971; Cruden, 1974; Franklin, 1971; Robertson, 1955; Schock and Heard, 1974; Walton, 1958; and Wawersik and Fairhurst, 1970). However, we are still severely limited in predicting the behavior of rock under crustal conditions because experimental data cannot be obtained on geologic dimensions or time scales. A predictive capability requires development of a general theory of the mechanical behavior of rocks.

Griffith (1921, 1924) postulated that materials contain cracks and stress is concentrated at crack tips when the material is stressed. When the stress at a crack tip exceeds the stress necessary to break atomic bonds in the crystal (theoretical strength) the crack propagates resulting in failure of the material. Griffith's theory predicts that the applied stress at failure should be less than the theoretical strength, that strength should increase with confining pressure, and that fracture should occur by the propagation of a single crack through the material. Although Griffith's idea of relating brittle fracture to crack growth is generally accepted, Griffith's theory fails to predict observed dilatancy before failure (Brace et al., 1966) or behavior of cracks subsequent to initial crack growth (Brace and Bombolakis, 1963).

McClintock and Walsh (1962) modified Griffith's analysis

on the basis of a model in which cracks close under pressure. Frictional stresses along the surfaces of closed cracks tend to resist additional deformation of the crack. Therefore, the stress concentration near crack tips will be less than for a similar crack whose walls are not in contact. The McClintock-Walsh modification predicts higher failure strength than Griffith's theory and dilatancy prior to failure. Strengths predicted by McClintock and Walsh fit many experimental observations if the coefficient of friction for crack surfaces is taken as unity. The coefficient of friction depends on crack surface characteristics and crack closure pressure. The coefficient of friction is not well known for cracks. Microscopic studies show that crack surfaces and morphologies can be quite variable even within a single rock (Simmons and Richter, 1974). Therefore, it is unlikely that the coefficient will be unity for all rocks.

Peng and Johnson (1972) predicted failure strength on the basis of beam buckling theory. They assumed that material fails due to the coalescence of en eschelon cracks. The material between each crack is treated as a beam and the body fails when the beams are strained in excess of the fiber strain of the material. The model depends upon the length to width ratio of the beams, the inclination of en eschelon cracks, the friction angle among beams, and the fiber strain which is non-linear with respect\* to stress. None of these parameters is independently well known for rocks, so any of a number of theo-

retical curves can be made to fit experimental data.

None of the proposed theories has universal applicability, but they all contain assumptions about the behavior of microcracks. Therefore, prior to development of a general theory for rock failure, we must determine the effects of cracks on rock failure. We have chosen to characterize cracks in several crustal igneous rocks that are produced by stressing in the laboratory (Chapter 3). Characterization of stress-induced cracks (SIC) includes determination of their morphology, distribution, abundance, and orientation. The effects of hydrostatic pressure cycling and uniaxial stress cycling are examined in Chapter 4, and we apply our laboratory results to the analysis of a 1.5 km deep granite core from Shannon County, Missouri in Chapter 5.

The cracks in rocks can be examined indirectly through their effects on various physical properties or directly with the petrographic microscope (PM) and scanning electron microscope (SEM). Measurements of such elastic properties as compressibility and velocities of compressional and shear waves are particularly useful because of their high sensitivity to open microcracks. For example, the compressibility of Westerly granite decreases about 70 percent between pressures of zero and two kilobars due to the closure of microcracks (Brace, 1965). The velocities of compressional and shear waves in dry samples and of shear waves in saturated samples of Westerly granite increase 15 to 60 percent between pres-

tures of zero and two kilobars (Birch, 1960; Nur and Simmons, 1969a).

Both optical and electron microscopes have been used for observing microcracks. Sprunt and Brace (1974) showed that the SEM could be used to examine open microcracks in rocks with a resolution of about  $10^{-5}$  cm. They studied cracks and pores in several rocks and showed that open cavities in many rocks have a wide range of lengths and of aspect ratios, and that most microcracks are one-tenth the grain size in length and up to 1  $\mu$ m wide. Simmons and Richter (1976) developed techniques for making 100  $\mu$ m thick sections of rocks without producing new cracks which could be studied with both the SEM (with the advantage of very high magnification and the possibility of determination of composition with energy dispersive x-ray systems) and the usual petrographic microscope (with its advantages of three-dimensional capabilities and ready mineral determination).

The primary methods used in this study for characterizing SIC are differential strain analysis (measurements of strain with high precision,  $\pm 2$  or  $3 \times 10^{-6}$ , versus hydrostatic pressure) and direct observations using the PM and SEM. Our purpose is threefold: (1) to understand the effects of stress on rocks more fully, (2) to provide a basis for interpreting anomalous changes in measured physical properties premonitory to earthquakes, and (3) to determine in situ stress states from analysis of SIC in rocks.

## CHAPTER 2

## EXPERIMENTAL CONSIDERATIONS

The Samples

The rocks examined consist of several granites, a gabbro, and a diabase. Sample locations are shown in Figure 2-1. Modal composition of the samples is determined by point counting and is listed in Table 2.1. The cracks in many of the rocks used in this study have been examined by other workers. References to these studies and petrographic descriptions of the samples are listed in Table 2.2.

Sample Preparation

Crack sections for microscopic examination were prepared without producing new cracks. Richter and Simmons (1977a) describe the procedure: blocks or cores (ca. 2 x 2 x 4 cm or 1.8 dia. x 2 cm) were cut with standard rock saws or coring equipment from rock in the central portion of the stressed cores. We then removed at least 6 mm of our sample with a Buehler Isomet saw rotating at a very slow speed (perhaps 30-50 rpm) to remove damaged rock. The Isomet-cut-face was ground by hand on glass plates to remove an additional 1-2 mm, polished to 0.05 $\mu$ m abrasive on a microcloth, and mounted on a glass slide with a room temperature curing epoxy. An Isomet was used to cut the remainder of the mounted slice to 2 mm. The section was then ground by hand to 100 $\mu$ m on glass

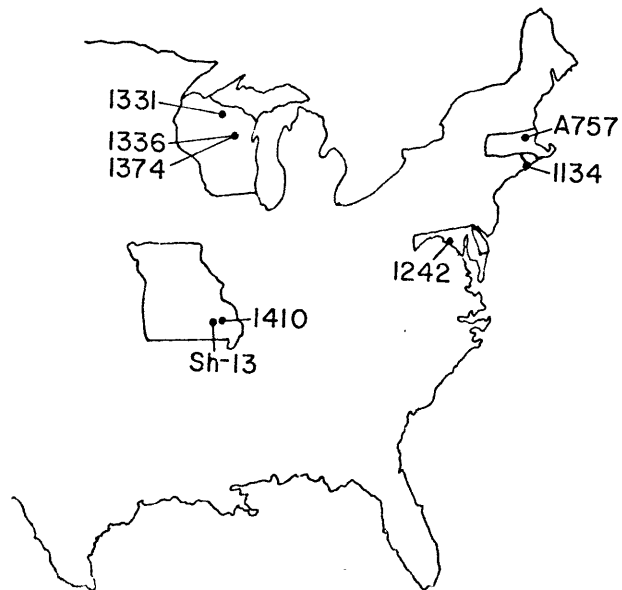


Figure 2-1. Location map for rocks examined in this study.

Table 2.1  
Modal Analysis

Mineral	A757 <sup>1</sup>	1134	1242	1331	1336	1410	1643 <sup>2</sup>
Plagioclase	18.5	39.2	47.3	53.7	23.8	26.9	33
K-Feldspar	36.3 <sup>3</sup>	30.7 <sup>3</sup>			44.8 <sup>4</sup>	39.3 <sup>4</sup>	32 <sup>5</sup>
Pyroxene			46.9	30.1			
Quartz	34.4	22.5			28.9	32.8	26
Olivine			0.4	1.1			
Biotite	0.9	5.0	0.8				8
Muscovite	8.4						
Opaque	0.1	0.7	2.5	3.1	1.0	tr	
Epidote	0.6						
Apatite	0.4				tr		
Secondary	0.4	0.4	2.2	12.2	1.5	0.5	
Others	tr <sup>6</sup>	1.5 <sup>7</sup>				tr <sup>8</sup>	1 <sup>9</sup>
Total	100.0	100.0	100.1	100.2	100.0	99.5	
Number of counts	8550	1000	1000	1000	1000	1200	



Table 2.1 (continued)

---

<sup>1</sup>Averaged from three orthogonal sections.

<sup>2</sup>Analysis from Council (1954).

<sup>3</sup>Microcline.

<sup>4</sup>Perthite

<sup>5</sup>Orthoclase.

<sup>6</sup>Zircon, carbonate, garnet.

<sup>7</sup>Apatite, muscovite.

<sup>8</sup>Fluorite, muscovite.

<sup>9</sup>Apatite, zircon, muscovite, chlorite, epidote.

Table 2.2

## Sample Descriptions

Name	Sample Number	Locality	Petrographic Description	Other Crack Studies	Geology References
Chelmsford (MA) granite	A757	Chelmsford, MA. Middlesex Co.	Medium grained (1-4 mm) granite. Slightly porphyritic hypidiomorphic granular texture, bluish-gray color, contains both biotite and muscovite.	Cooper and Simmons (1977) Richter and Simmons (1977b) Simmons and Richter (1974)	Dale (1923) Skehan (1967)
Westerly (RI) granite	1134	Crumb quarry 1 mi SE of Bradford RI, 1/4 mi E of Ross Hill Rd., Washington Co.	Fine grained (0.3-1.0 mm) massive quartz monzonite. Bluish-gray color. Mainly composed of oligoclase, quartz, microcline, and biotite. Minor alteration of feldspars to clays and biotite to chlorite.	Cooper and Simmons (1977) Feves and Simmons (1976) Feves <u>et al.</u> (1977) Richter and Simmons (1977b) Siegfried and Simmons (1977)	Dale (1923) Quinn (1943) Skehan (1967)
Frederick (MD) diabase	1242	1 mi N of Mt. Pleasant (MD), at intersection of Crum Rd. and Stauffers Rd. Frederick Co.	Fine grained (0.1-0.5 mm) olivine diabase with intersertal to subophitic texture.	Simmons and Cooper (1977) Simmons and Richter (1974) Siegfried and Simmons (1977)	Anna and Stose (1946)

Table 2.2 (continued)

Name	Sample Number	Locality	Petrographic Description	Other Crack Studies	Geology References
Mellen (WI) gabbro	1331	WI highway 13, 2.1 mi S of intersection with WI highway 77, NW 1/4, sec 6, T43W, R2E, Ashland Co.	Fine grained (0.2-0.5 mm) massive ophitic olivine gabbro.		Tabet (1974)
Wausau (WI) granite	1336 1374	Prehn quarry, Wausau, SE 1/4, sec 9, T30N, R7E, Marathon Co.	Medium grained (1-3 mm) even textured 'dry' granite composed of quartz, perthite, plagioclase. Very few mafic minerals	Cooper and Simmons (1977) Feves <i>et al.</i> (1977) Richter and Simmons (1977a)	Lockwood (1970)
Graniteville (MO) granite	1410	Abandoned quarries 30 meters E of MO highway 21; NE 1/4, sec 10, T34N, R3E, Iron Co.	Medium grained (1-4 mm) massive granite with few mafic minerals.		Tolman and Robertson (1969)
Mt. Airy (NC) granite	1643	Surface quarry of N. Carolina Granite Corp. 3 mi S of Mt. Airy, N.C. Surry Co.	Medium grained (1-4 mm) 'white' even-textured granite. Mainly composed of feldspar, quartz, and biotite. Minor kaolinization of feldspar.		Winkler (1973) Council (1954) Stuckey and Conrad (1958)

Table 2.2 (continued)

Name	Sample Number	Locality	Petrographic Description	Other Crack Studies	Geology References
Missouri granite core	Sh-13	NW 1/4 SW 1/4 SW 1/4, sec 28, T31N, R4W, Shannon Co.	Medium grained (1-4 mm). Primarily composed of quartz and perthite with myrmekitic texture. Alteration is disseminated at shallow depth, and is more concentrated along cracks at greater depths.		Kisvarsanyi (1975) Tolman and Robertson (1969)

plates and polished to 0.05 $\mu$ m abrasive on a microcloth. Approximately 10-15 microns of material were removed from each section by ion bombardment and the samples were coated with ~500 $\text{\AA}$  of gold. The ion milling removes polishing damage, produces slight topography among the minerals, and also produces the elliptical mounds evident in the figures. Because crack sections are three times as thick as standard thin sections, cleavage cracks and other introduced cracks are not formed during sample preparation. Microcracks in crack sections prepared in this way can be examined with both the SEM and petrographic microscope.

Samples used for differential strain analysis were also cut from the central portion of the stressed cores. Three orthogonal faces were ground using 120, 220, 400, and 600 grit silicon-carbide abrasive and a cast iron rotating lap. Electrical resistance foil strain gages (BLH Co. Type FAE) were mounted to these surfaces with a room temperature curing epoxy (Tra-Con 2101), and all samples were dried in a vacuum of  $10^{-5}$  torr. Some samples were left in the vacuum at room temperature for 10 days. Other samples were heated at a rate less than 15 $^{\circ}$ C/hr to 40 $^{\circ}$ C or 250 $^{\circ}$ C in the vacuum. Additional cracks can be caused by heating to 250 $^{\circ}$ C - both thermal gradient cracks and thermal cycling cracks (Simmons and Richter, 1976). The low heating rate was chosen to minimize the production of thermal gradient cracks (see Richter and Simmons, 1974). The additional cracks produced by thermal cycling to

250°C can be measured and the data on cracks present in stressed samples can be corrected for their presence. All samples were then encapsulated in Dow Corning Sylgard 186, a translucent and impermeable elastomer, to exclude the pressure medium from the cracks in the sample.

### Uniaxial Stressing

Several cores 2.54 cm in diameter and 8 to 12 cm long were cut from each sample block. All blocks were labeled with orthogonal reference axes A, B, and C, and each core was cut with the core axis parallel to either A, B, or C. The core axis was parallel to the rift plane for samples 1134 and 1643. All other samples did not contain a pronounced rift plane as indicated by an isotropic initial crack distribution. Core orientations for all samples are listed in Table 2.3. The ends of each core were ground parallel and flat to 25 $\mu$ m with a surface grinder before stressing.

During stressing, the acoustic emissions (AE) of each sample were monitored. Our AE system is similar, but not identical, to several other systems (Scholz, 1967; Hardy, 1972; Knill et al., 1968; Mogi, 1968; and Todd, 1973). The acoustic pulses are detected with a lead-zirconate-titanate piezoelectric transducer, amplified, filtered, and admitted to a Hewlett Packard HP H22 5401B pulse height analyzer with 1024 channels of memory. The multichannel analyzer is operated in multichannel scaling mode with a dwell time of 10

seconds per channel. Applied stress was continuously recorded using a load cell and strip chart recorder. The load rate was between 100 and 150 bars per minute for all samples except 1134 where the load rate was less than 10 bars per minute. Sample configuration and AE apparatus are shown schematically in Figure 2-2. Maximum stress for each sample is listed in Table 2.2.

Typical plots of the rate of AE(N) and stress versus time are shown in Figure 2-3. Qualitatively, these plots show the same features as observed by many investigators (Obert and Duvall, 1945; Mogi, 1962; Scholz, 1968). Namely, a peak is present in the AE spectrum at low stress which depends upon initial porosity and is attributable to the closing of microcracks. At high stress, there is a large sudden increase in the rate of AE just prior to failure.

It has been recognized, at least since 1902, that measured rock strength is related to such experimental conditions as sample geometry, end loading conditions, strain rate, and confining pressure (Filon, 1902; Brace, 1964; Mogi, 1966; Peng and Johnson, 1972). By uniaxially stressing cores of various dimensions, Obert et al. (1946) found that the strength,  $C$ , is related to sample geometry by:

$$C = C_0 \left( 0.778 + 0.222 \frac{D}{L} \right) \quad (2.1)$$

where  $C_0$  is the measured strength when the diameter ( $D$ ) equals the length ( $L$ ). For our samples  $0.2 < \frac{D}{L} < 0.5$ , and

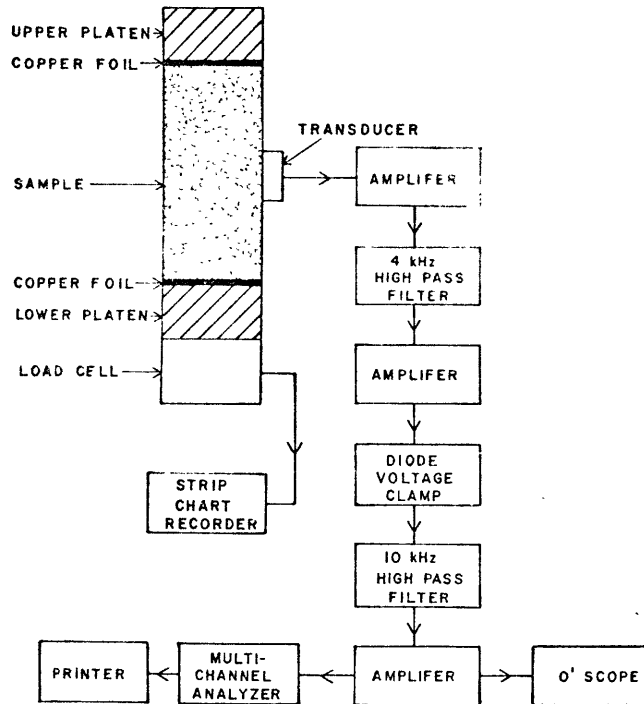


Figure 2-2. Block diagram of apparatus used to monitor acoustic emissions and stress. Each amplifier provides either 20 db or 40 db of gain. The multichannel analyzer is operated in multichannel scaling mode. Copper foil is placed between the sample and loading platen to reduce end effects.



Table 2.3  
Maximum Uniaxial Stress

Sample	Core Axis	Peak Load (bars)
1134-1	B	930
1134-2	B	1770
1134-3	B	1815
1134-6	B	1890
1134-7	B	0
1134-8	B	1930
1134-9	B	1930
1134-13	B	1600
1134-15	B	0
1134-16	B	0
1134-17	B	1755
1134-18	B	1160
1134-19	B	1975
1134-20	B	0
1242-2	B	3430
1242-3	B	3840
1242-5	B	3720
1242-6	B	3700
1242-15	B	0
1331-0	C	0
1331-4	C	4270
1331-5	C	2870

Table 2.3 (continued)

Sample	Core Axis	Peak Load (bars)
1336-0		0
1336-4	B	2580
1336-5	B	2530
1336-6	B	2060
1410-0	B	0
1410-1	B	2375
1410-2	B	2030
1410-3	B	2420
1643-1	A	0
1643-2	A	1600
1643-3	A	1650
1643-4		0
1643-5	A	1480

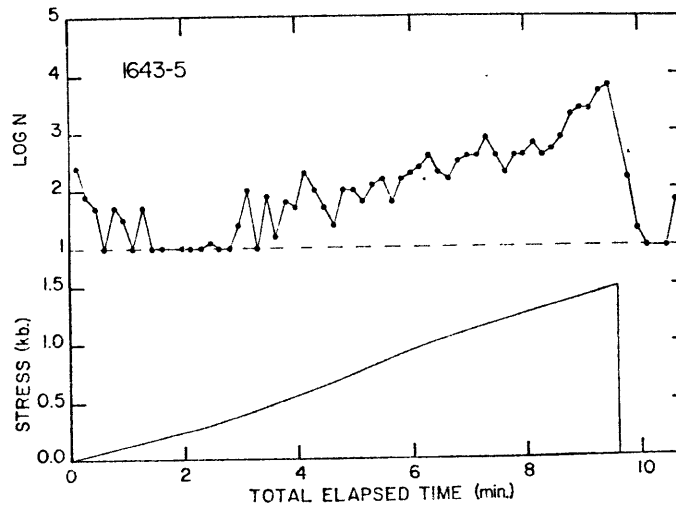
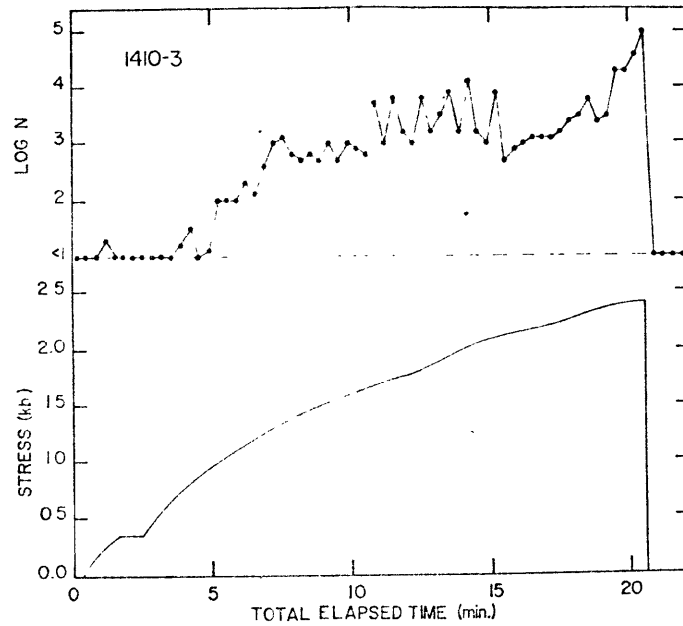


Figure 2-3. Number of acoustic emissions (N) per 10 second interval and applied stress versus time. The acoustic emission peak at low stress is due to the closing of cracks. Failure is usually preceded by a large sudden increase in N.

C varies by less than one percent. Therefore, we assume that variations in our sample length will have negligible effect on measured strength.

A mismatch in elastic properties between the rock sample and the steel loading platen may also cause variations in measured strength. This mismatch results in radial shearing stresses at the interface. For most rocks, these stresses act inward to produce a 'clamping effect' which does two things. First, a stress concentration arises at the outer edge of the steel-rock interface due to the abrupt change in shearing stress there. This stress concentration would tend to lower the apparent strength. Second, if a fracture propagates into the region near the end of the sample, growth of the fracture may be impeded. This effect would increase the apparent strength. In order to reduce end effects, we placed copper foil between the sample and platen and used platens of the same diameter as the sample. Visual examination of our stressed samples indicated that microcracks penetrated only one or two centimeters into the samples from the ends due to the first effect. We removed three to four centimeters of material from each core end and assumed that the stress was uniform in the remaining portion. This assumption is probably valid except in the final stages of stressing when some samples showed signs of material flaking from the midportion. Flaking reduces the cross-sectional area and thereby increases the stress.

### Differential Strain Analysis

Strain was measured as a function of hydrostatic pressure with differential strain analysis (DSA). Complete details of the DSA technique and its theoretical basis can be found in Simmons et al. (1974), Siegfried and Simmons (1977) and Siegfried (1977). For completeness we include a brief overview of DSA adopted from Feves et al. (1977). In DSA, we measure strain in materials to very high precision,  $\pm 2$  or  $3 \times 10^{-6}$ . High precision is obtained with a simple trick: the measured strain of a reference sample of fused silica is subtracted from the measured strain of a rock, measured at the same time and under identical conditions. A graphical representation of a DSA compression curve is shown in Figure 2-4. In Figure 2-4a, the dashed line represents the linear strain measured as a function of pressure for a fused silica reference and the solid line represents the strain of a typical cracked solid. If we subtract the strain of the fused silica from the strain of the cracked solid, we obtain the curve in Figure 2-4b which is the DSA differential strain curve.

If we assume that the compressibility of fused silica is constant for pressures below 2 kbar, we have

$$\hat{\epsilon} = \epsilon + P\beta_{FS} \quad (2.2)$$

where  $\hat{\epsilon}$  is the differential strain,  $\epsilon$  is the measured rock strain at pressure  $P$ ,  $\beta_{FS}$  is the fused silica compressibility,

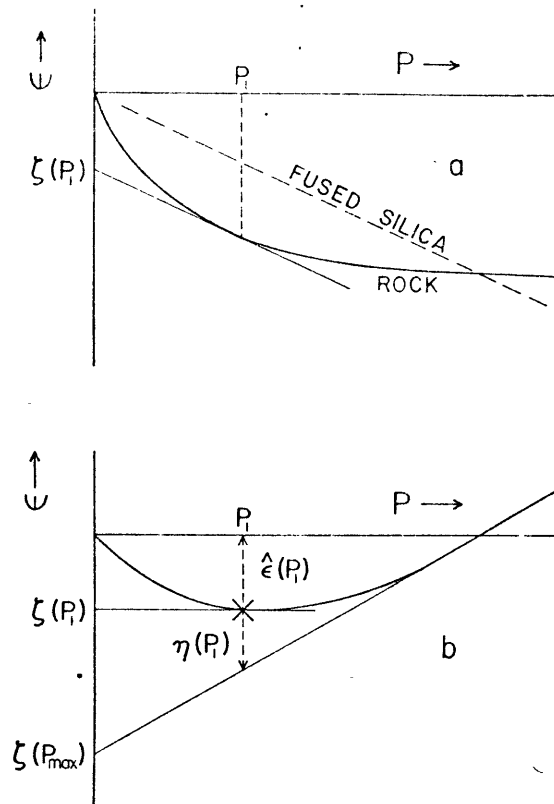


Figure 2-4. Components of DSA curve. In Figure 2-4a, the measured strain of the fused silica reference (dashed line) is subtracted from the measured strain in a rock (solid line) to yield the DSA compression curve in Figure 2-4b. The zero pressure intercept,  $\zeta(P_1)$ , of a line tangent to the strain curves at any pressure,  $P_1$ , is the strain at zero pressure associated with cracks which have completely closed by pressure  $P_1$ . Here,  $\eta(P_1)$  is the total open crack porosity at  $P_1$ . (See text for details.)

and we use the convention that compressive strains are negative. In our previous work (Simmons et al., 1974; Simmons et al., 1975), we assumed constant  $\beta_{FS}$ ; however, in the present work, we have corrected for the fused silica compressibility pressure dependence using the data of Peselnick et al. (1967). Their measurements show that the linear compressibility of fused silica varies from  $0.913 \times 10^{-6} \text{ bar}^{-1}$  at  $P = 0$  to  $0.945 \times 10^{-6} \text{ bar}^{-1}$  at 2 kbar. The actual sample strain is calculated by adding to the differential strain the fused silica strain calculated from Peselnick's data. Then, in order to expand the strain scale on plots, and to facilitate comparison with previous differential strain data, a linear strain curve with a slope equal to the zero pressure fused silica compressibility determined by Peselnick et al. is subtracted from the actual strain curve. Thus, the differential strains in this paper can be converted to true strains with the formula:

$$\epsilon = \hat{\epsilon} - P\beta \quad (2.3)$$

where  $\beta = 0.913 \times 10^{-6} \text{ bar}^{-1}$ .

The DSA compression curve is related mathematically to the cracks present in the sample. In a crack-free solid, the curve is a straight line with a slope given by the difference in compressibilities of the sample and fused silica. But for a sample containing cracks the strain at pressure  $P = 0$  due to cracks which are completely closed by pressure  $P_1$ , denoted

by  $\zeta(P_1)$ , is given by the expression

$$\zeta(P_1) = P_1 \left. \frac{d\hat{\epsilon}}{dP} \right|_{P_1} - \hat{\epsilon}(P_1) \quad (2.4)$$

where  $\hat{\epsilon}$  is the linear differential strain. Equation 2.4 has a simple geometrical interpretation. From Figure 2-4,  $\zeta(P_1)$  is seen to be the zero pressure intercept of a line tangent to the strain curve (and also the differential strain curve) at  $P_1$ . The linear crack porosity due to all cracks that remain open at  $P_1$  is also shown and may be expressed as

$$\eta(P_1) = \zeta(P_{\max}) - P_1 \left. \frac{d\hat{\epsilon}}{dP} \right|_{P_{\max}} + \hat{\epsilon}(P_1) \quad (2.5)$$

where  $\hat{\epsilon}(P_1)$  is the value of differential strain at  $P_1$ . If the strains of Figure 2-4 are volumetric strain, then we obtain  $\zeta_v(P)$  which is the volumetric strain at  $P = 0$  due to all cracks that close at  $P \leq P_1$  and  $\eta_v(P_1)$  which is the (usual) volumetric crack porosity at  $P_1$ . Note that  $\eta_v(0)$  is the crack porosity that has been used previously by other authors (e.g., Walsh, 1965; Todd et al., 1973a).

In addition to crack porosity as a function of pressure, DSA allows us to obtain the distribution of crack porosity (at  $P = 0$ ) with respect to the crack closure pressure, termed crack spectrum, and the effective orientation of the cracks associated with each value of crack closure pressure. Morlier (1971), based upon the work of Walsh (1965), showed that compression curves can be interpreted in terms of the distribution of crack aspect ratios. Siegfried and Simmons (1977)



replaced the penny-shaped or elliptical crack models of Morlier and Walsh with the assumption that strain is linear over any pressure range in which no cracks close completely. They obtained:

$$v(P) = P \left( \frac{d^2 \hat{\epsilon}}{dP^2} \right) \quad (2.6)$$

where  $v(P)dP$  is the strain at zero pressure due to the presence of cracks closing between  $P$  and  $dP$ . We therefore can determine crack spectra by twice differentiating strain curves. Without the high precision data obtained with DSA, it would not be possible to obtain meaningful results from these differentiations.

## CHAPTER 3

## CHARACTERIZATION OF LABORATORY STRESS-INDUCED CRACKS

Introduction

The study of stress-induced cracking is of great importance to the understanding of the behavior of rocks in tectonically active zones (Brace et al., 1966; Scholz et al., 1973; Mjachkin et al., 1975). In previous laboratory studies of stress-induced cracks (SIC), crack characteristics were inferred from electrical or elastic measurements (Matsushima, 1960; Nur and Simmons, 1969a; Brace and Orange, 1968) or from direct observations with the petrographic microscope (Paulding, 1965; Friedman et al., 1970; Wawersik and Brace, 1971; Peng and Johnson, 1972; Hallbauer et al., 1973). Recently, Tapponnier and Brace (1976) have examined stress-induced cracks (SIC) with the SEM.

None of these methods yields a complete characterization of cracks. Electrical and elastic measurements yield only some averaged crack property. The petrographic microscope has very limited resolution and many cracks are below this resolution (Sprunt and Brace, 1974). The SEM has a resolution of  $10^{-5}$  cm, but yields only a two-dimensional view. In order to obtain a complete characterization of laboratory stress-induced cracks we have combined observations with the SEM, PM, and differential strain analysis.

### Microscopic Observations

Observations with the petrographic and scanning electron microscopes show that many SIC are transgranular, they may cross many grain boundaries, they form parallel to subparallel sets, and they are typically planar. SIC can be either associated with pre-existing cracks or they may appear isolated in the plane of view.

In order to distinguish SIC from pre-existing crack features, we have examined several crack sections from unstressed rocks. Naturally occurring cracks are often confined to grain boundaries, have rounded terminations, and contain bridges. The sites of previously open cracks are often marked by planes of secondary fluid inclusions, sealed cracks, or healed cracks.

Examples of naturally occurring crack features are shown in Figures 3-1 to 3-5. Table 3.1 lists the abbreviations used for all micrographs. Figure 3-1 is an SEM mosaic of the Wausau granite. The open microcrack is discontinuous and has blunt terminations (BT). The two rows of holes are part of planes of fluid inclusions (FI), which mark the sites of previously open microcracks (Tuttle, 1949). Sometimes the fluid inclusions contain crystals which have grown after formation of the inclusion (see Figure 3-2).

A typical view of unstressed Westerly granite is shown in Figure 3-3. Many of the cracks are confined to grain boundaries and have blunt terminations. All cracks contain healing

Table 3.1

## List of Abbreviations

---

qtz	Quartz
plag	Plagioclase feldspar
ksp	Potassium feldspar
pert	Perthite
biot	Biotite
hbd	Hornblende
ilm	Ilmenite
SIC	Stress-induced crack
PHC	Partially healed crack reopened by stress
FI	Fluid inclusions which are part of a plane of inclusions and mark the site of a previously open crack
BT	Blunt termination of a partially healed pre-existing crack
NB	Narrow bridge
WB	Wide bridge

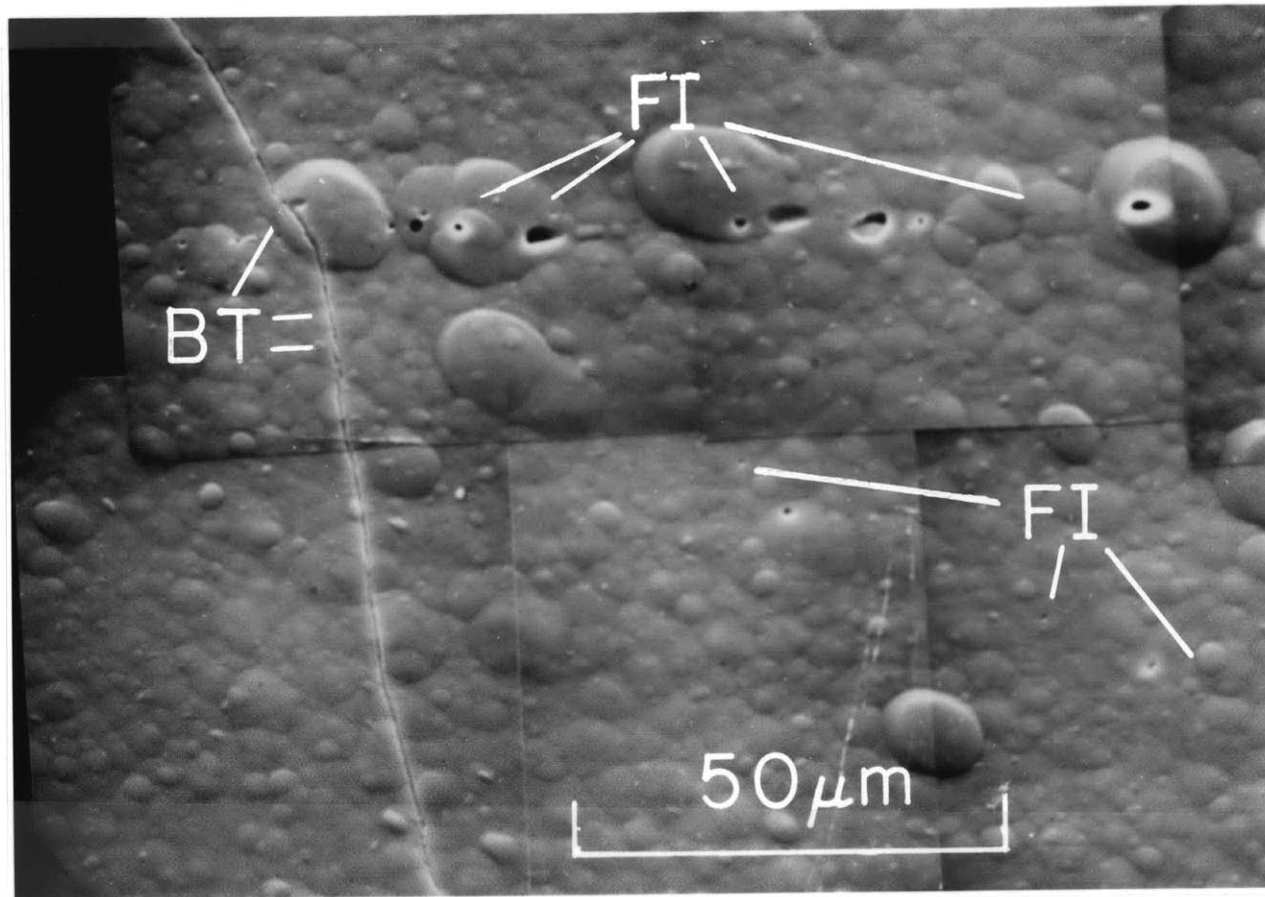


Figure 3-1. Microcracks in quartz, unstressed Wausau granite sample 1336-0. Open microcracks in unstressed samples are discontinuous and have blunt terminations (BT). The linear arrays of holes are the surface expressions of planes of fluid inclusions (FI), and mark the sites of previously open microcracks. SEM micrograph.

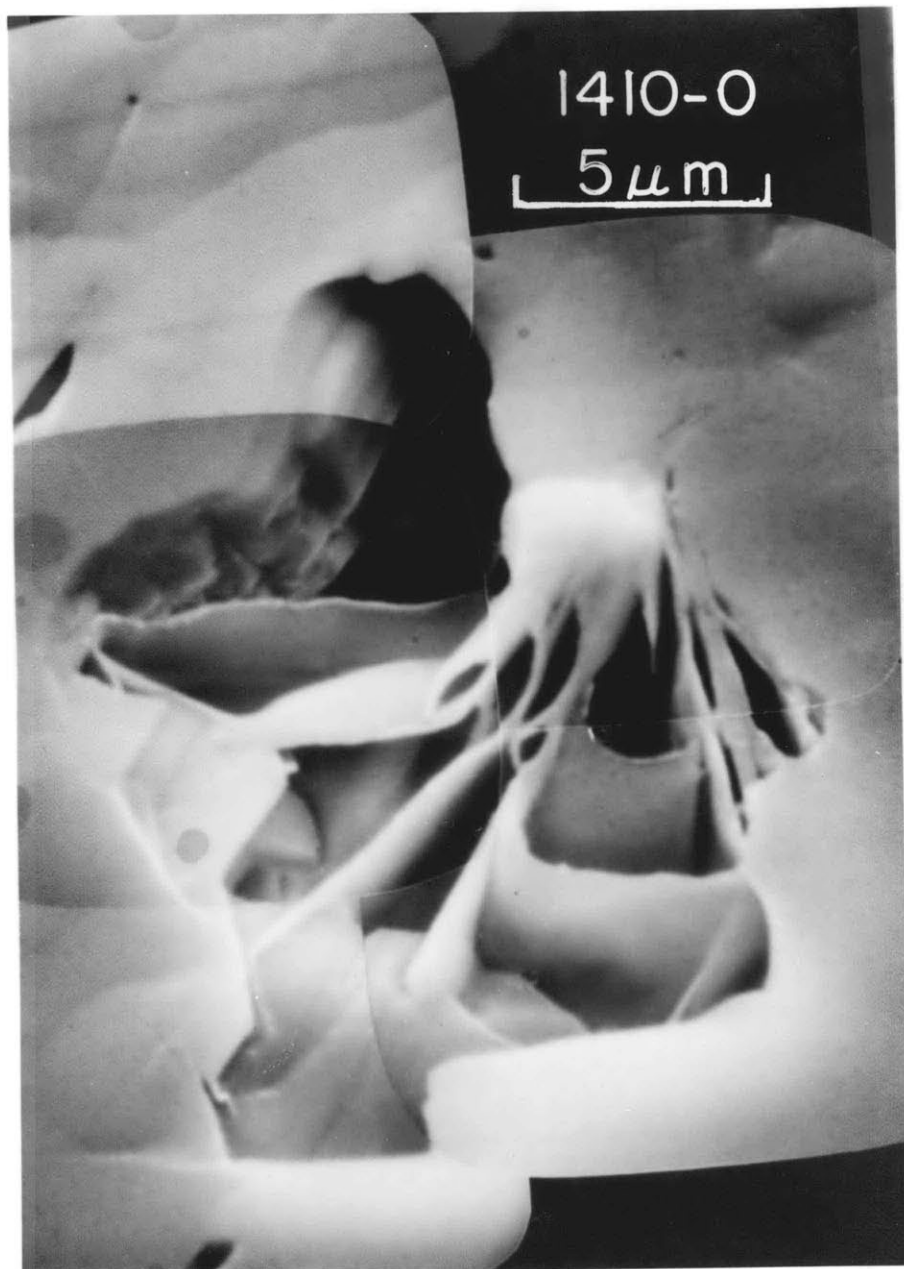
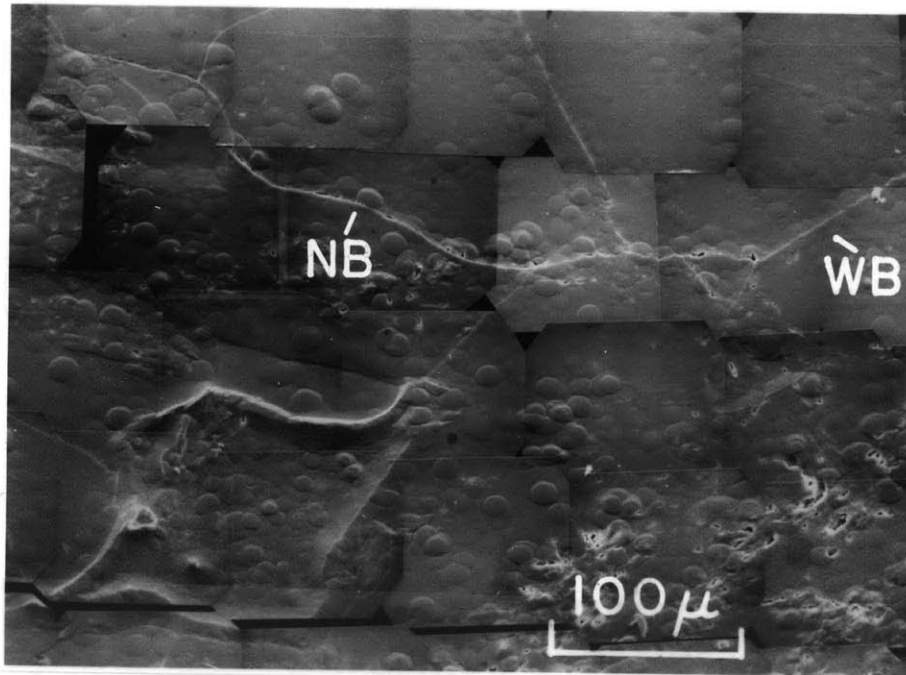
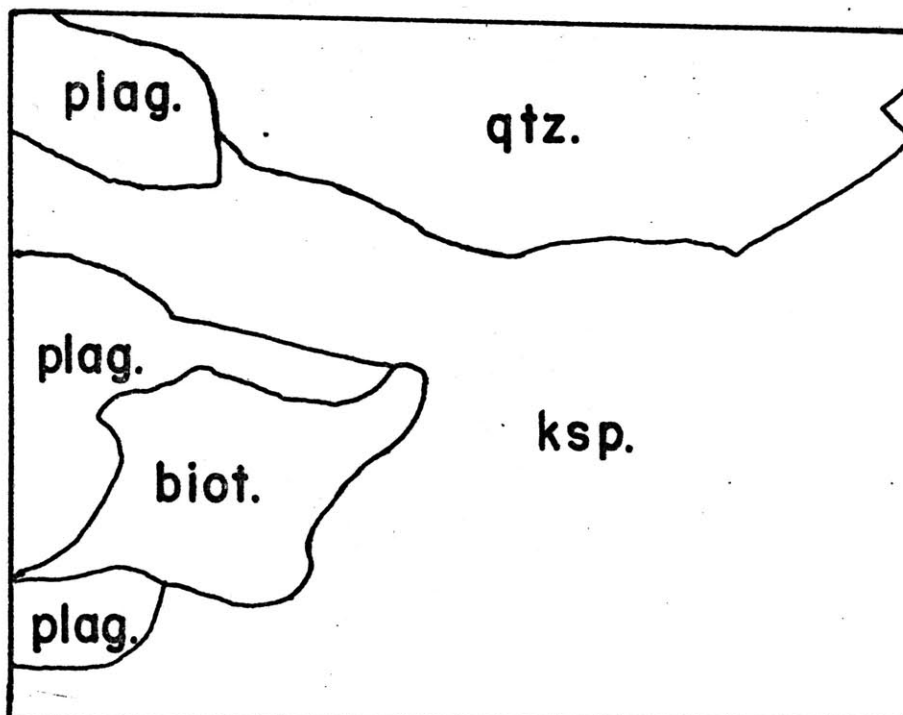


Figure 3-2. Growth of crystals in fluid inclusion in quartz. Graniteville granite sample 1410-0. SEM micrograph.



3-3a



3-3b

Figure 3-3. Typical texture of unstressed Westerly granite sample 1134-9. Most cracks are confined to grain boundaries and all cracks contain healing features. (3-3a) SEM micrograph. (3-3b) Mineral grain map.

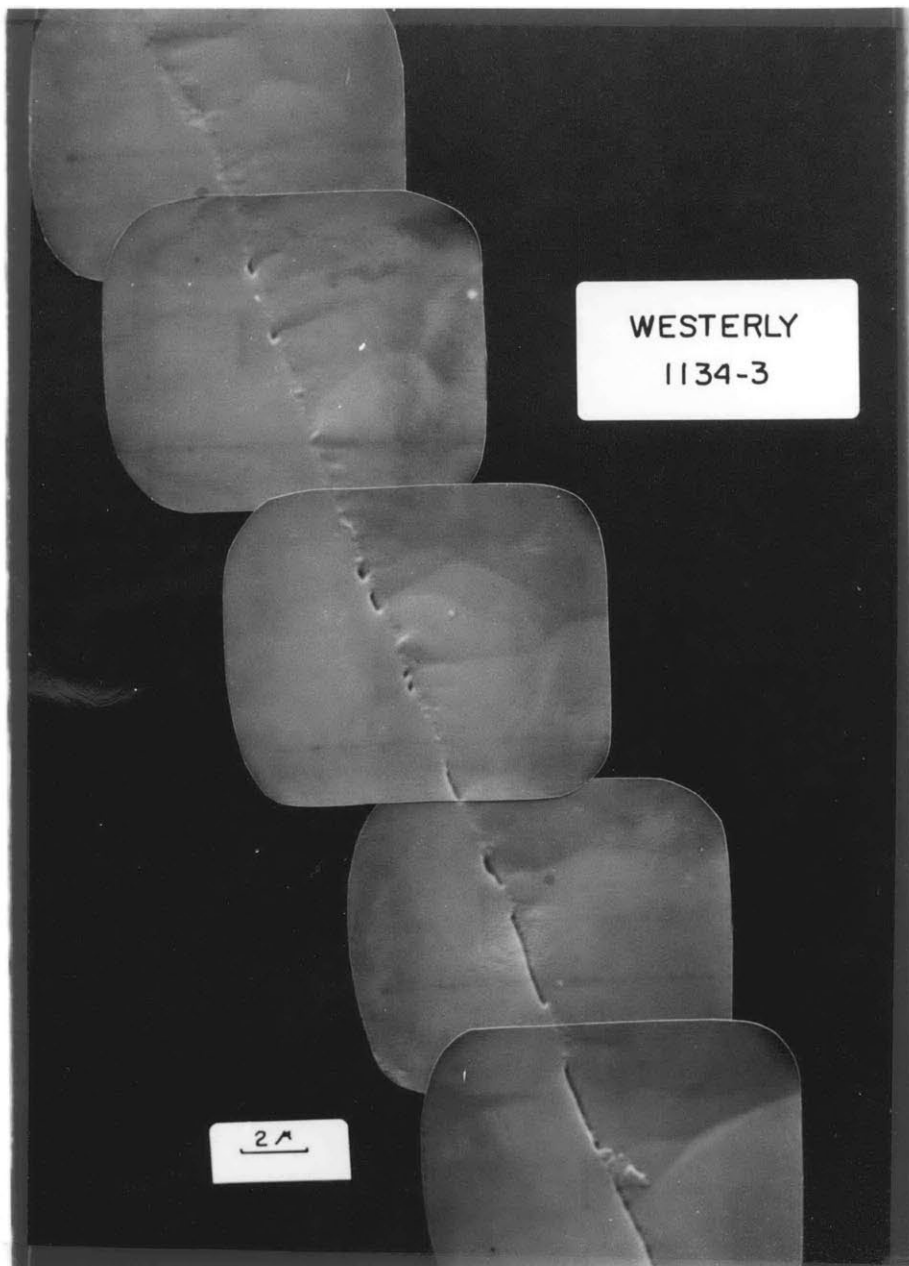
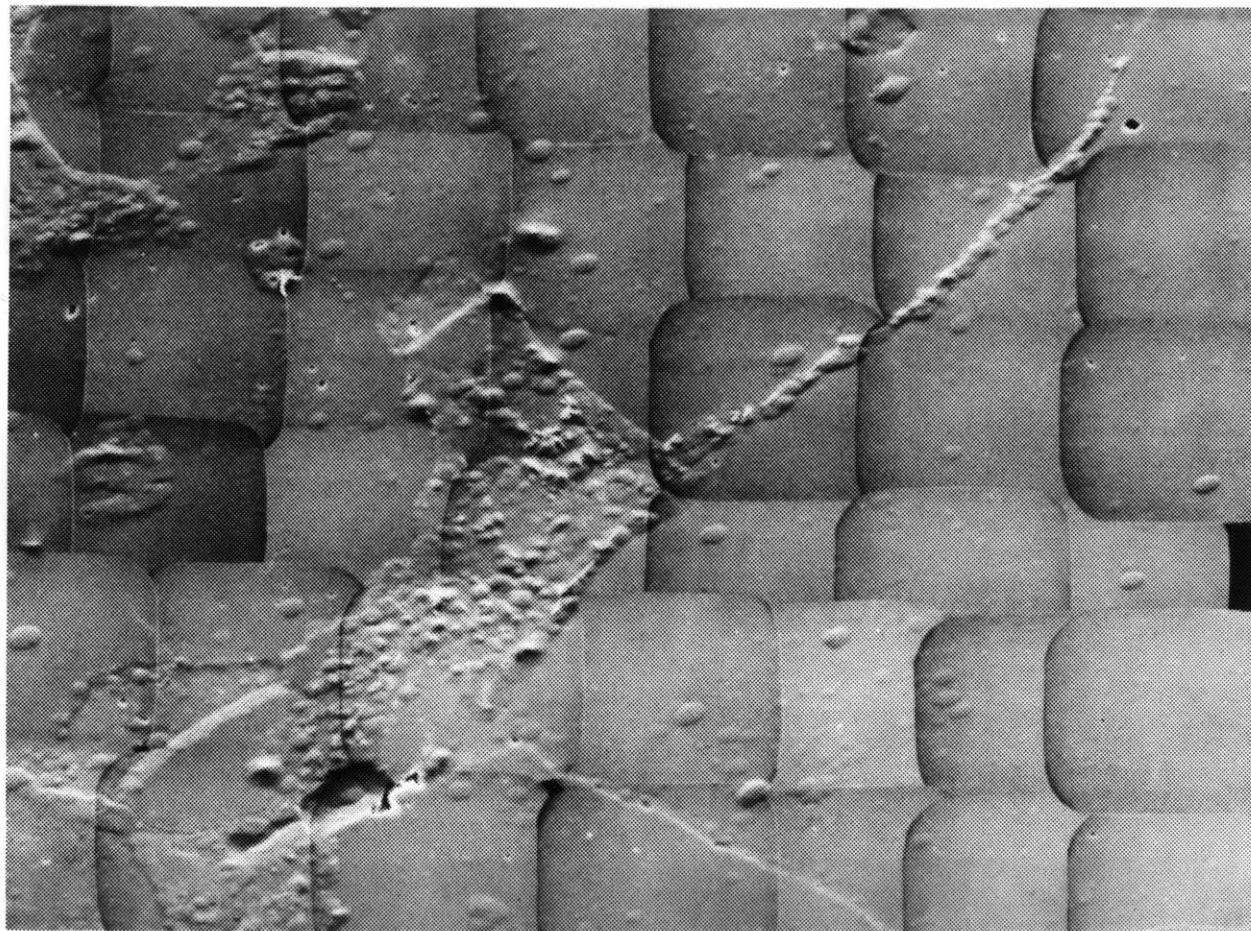


Figure 3-4. Partially healed crack in quartz, unstressed Westerly granite sample 1134-3. SEM micrograph.





100  $\mu$ m

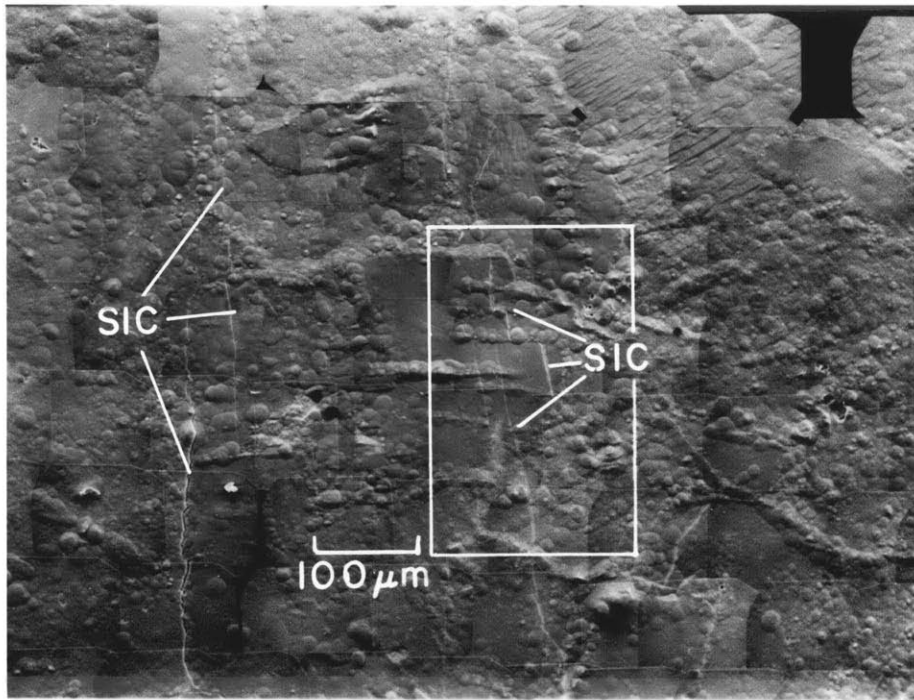
Figure 3-5. Typical texture of unstressed Graniteville granite sample 1410-0. The flat sparsely mounded areas are quartz; the highly mounded areas in the upper left and lower center are feldspar. The narrow strip of highly mounded material at the upper right is a feldspar sealed crack. SEM micrograph.

features along at least a portion of their length. Early stages of crack healing are represented by narrow bridges (NB). Further healing produces wider bridges (WB) which results in the formation of slot-like cavities (Figure 3-4), then holes (Figure 3-1), and finally total annealing of the crack.

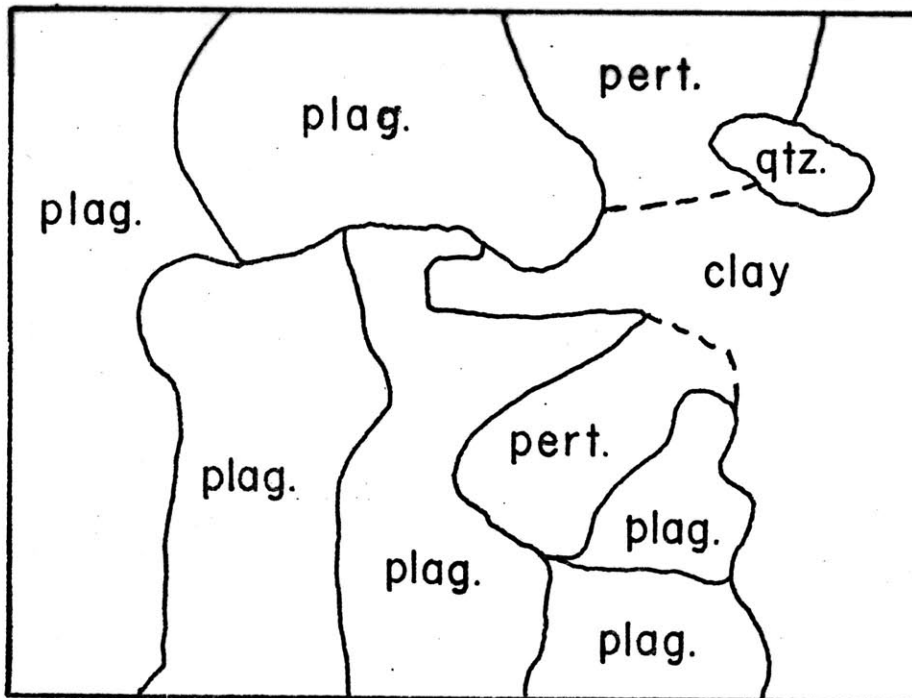
A typical view of unstressed Graniteville granite is shown in Figure 3-5. This rock contains many healed and sealed microcracks. The open microcracks occur most commonly along grain boundaries, but show no preferred orientation. They are generally 0.1-0.3 $\mu$ m wide with short segments that are completely healed. A complete description of Wausau and Graniteville granite can be found in Richter and Simmons (1977a).

In contrast to the crack morphologies shown in Figures 3-1 to 3-5, many cracks in laboratory stressed samples have sharp terminations and do not contain healing features. We infer that these 'fresh-looking' sharp ended cracks are stress-induced. Comparison of Figure 3-6, which is an SEM micrograph of stressed Graniteville granite, with Figure 3-5 shows the dramatic change in morphology due to stressing. Figure 3-6 contains many open stress-induced cracks. These transgranular cracks often form parallel sets and cross many grain boundaries with no change in orientation. They may be slightly offset at grain boundaries.

Another view of stressed Graniteville granite is shown in Figure 3-7. Here the SIC are associated with pre-existing



3-6a



3-6b

Figure 3-6. Typical texture for stressed samples. Graniteville granite sample 1410-2. SIC cross several grain boundaries with no change in orientation, some SIC are offset at grain boundaries. Maximum stress was normal to the plane of the section. (3-6a) SEM micrograph. (3-6b) Mineral grain map. (3-6c) Close-up of boxed area.

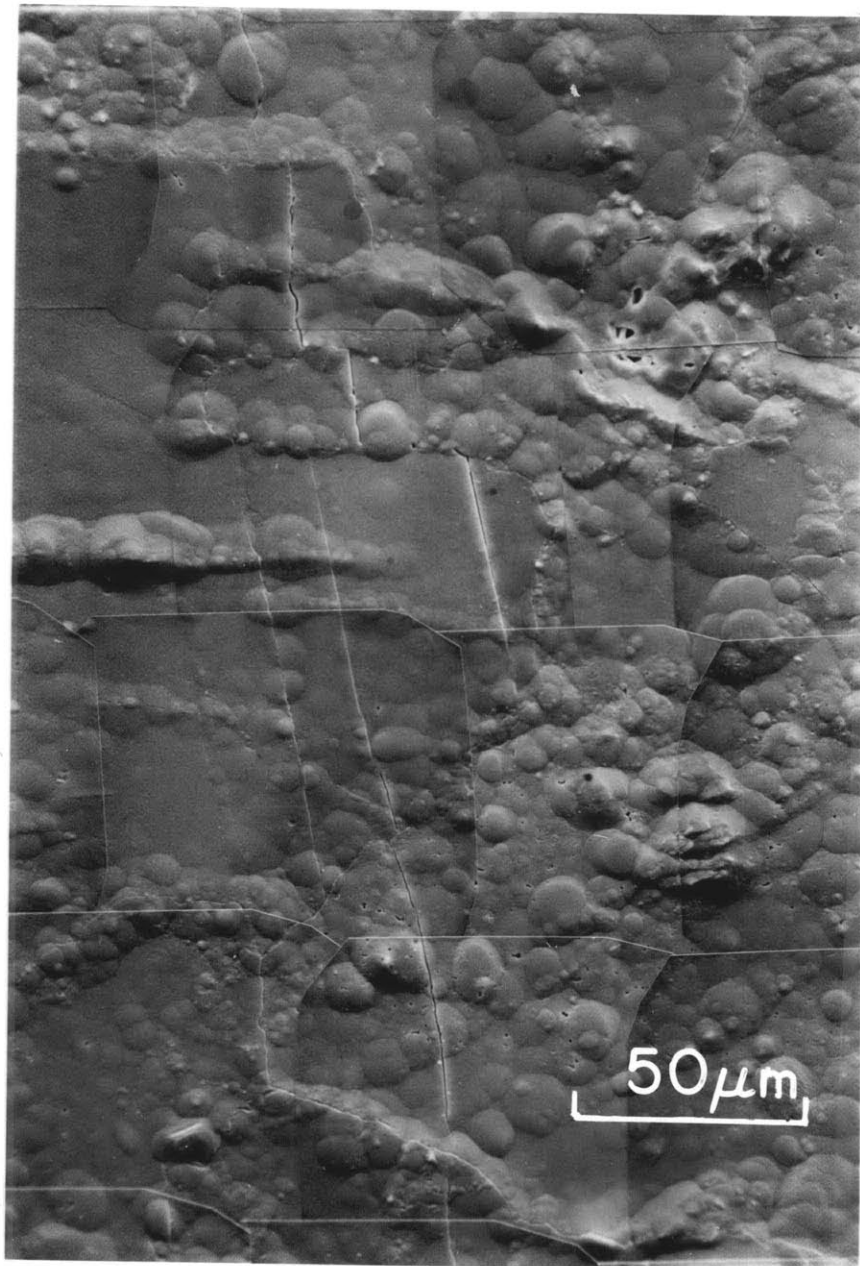
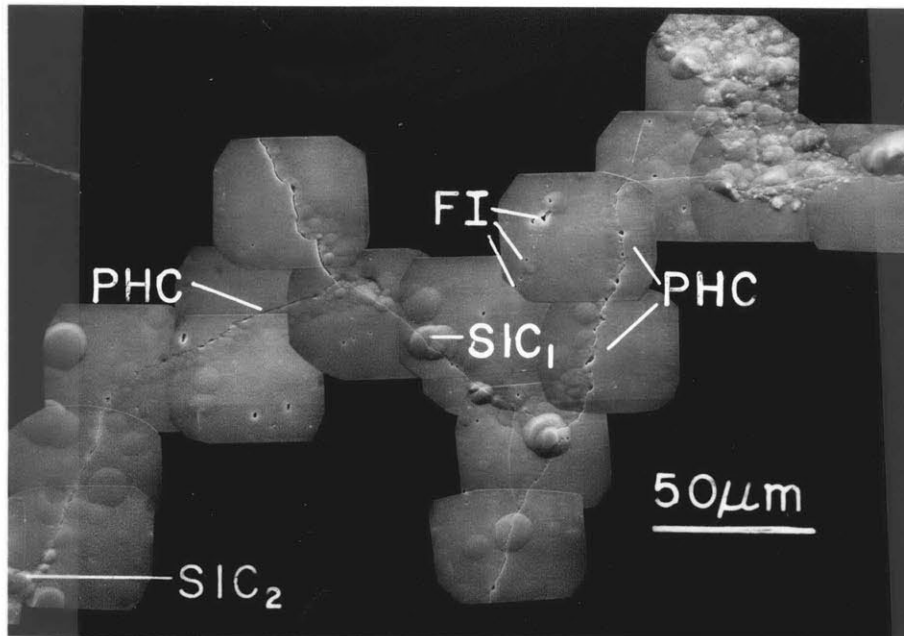
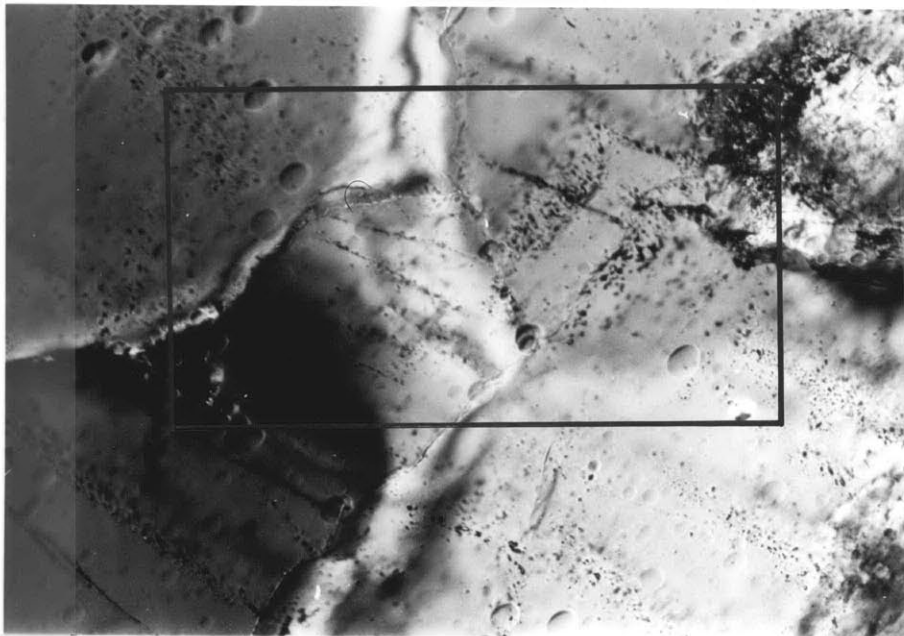


Figure 3-6c.



3-7a



3-7b

**Figure 3-7.** SIC associated with pre-existing cracks in stressed Graniteville granite sample 1410-2. Stressing has reopened partially healed quartz grain boundary cracks (PHC and SIC<sub>1</sub>). SIC<sub>2</sub> is a transgranular crack which does not appear to be associated with pre-existing cracks. Maximum stress was normal to the plane of the section. (3-7a) SEM micrograph. (3-7b) Plane polarized light. Figure 3-7a is outlined by the box.



Figure 3-8. Stress induced elongation of pre-existing crack in quartz. SIC are parallel to the direction of maximum compression. SEM micrograph of sample 1134-9.

cracks and fluid inclusion planes. The pre-existing crack with the blunt termination in the upper left corner may have provided a nucleation site for the stress-induced crack labeled SIC<sub>1</sub>. Partially healed cracks, labeled PHC, have been reopened by stress, but note that not all fluid inclusion planes have been reopened. The crack labeled SIC<sub>2</sub> is a transgranular stress-induced crack which is not associated with a pre-existing crack in the plane of view. SIC<sub>2</sub> could be associated with a pre-existing crack which is above or below the surface of the crack section.

Stress may modify pre-existing cracks in other ways. In Figure 3-8, stress has elongated the pre-existing crack. The apparent bridging of the crack at the junction of the SIC and pre-existing crack is due to electron charge accumulation and poor photographic resolution. Direct observation using the SEM cathode ray tube shows that the crack is continuous.

The characteristics of stress-induced cracks that can be seen with the scanning electron microscope and the petrographic microscope can be used to identify naturally occurring stress-induced cracks in rocks. We have used them to identify SIC in a set of cores from southeastern Missouri (see Chapter 5).

#### DSA Results

We have examined more than 100 DSA compression curves from both virgin and laboratory stressed rocks. Typical clo-



sure pressure spectra in three orthogonal directions for stressed and unstressed samples are shown in Figures 3-9 to 3-11. Volumetric crack distributions can be obtained by adding the three orthogonal distributions. Most crack spectra for stressed samples contain a pronounced peak between 100 and 200 bars. This peak is absent in most spectra from unstressed samples and indicates that the closure pressure of many SIC is between 100 and 200 bars. Mt. Airy granite (Figure 3-11) contains pre-existing cracks with closure pressure of about 150 bars and stressing increases the volume of 150 bar closure pressure cracks.

Stressing also increases the total crack porosity as shown by the increased area under the closure pressure curves for the stressed samples. The increase in crack porosity after stressing is the residual crack porosity after the stress has been removed and it is related to the pre-existing crack porosity. Figure 3-12 shows that stress-induced crack porosity increases with increasing pre-existing crack porosity. The data for Figure 3-12 are listed in Table 3.2. The line through the data in Figure 3-12 is a least squares fit and can be expressed as

$$\text{Log } (\Delta\zeta_v \times 10^6) = 0.69 \text{ Log } (\zeta_v^i \times 10^6) + 0.66 \quad (3.1)$$

The initial crack porosity,  $\zeta_v^i$  (2kb), is determined from separate unstressed\* samples which came from the same block as the stressed samples.  $\Delta\zeta_v$  (2kb) is obtained by subtrac-



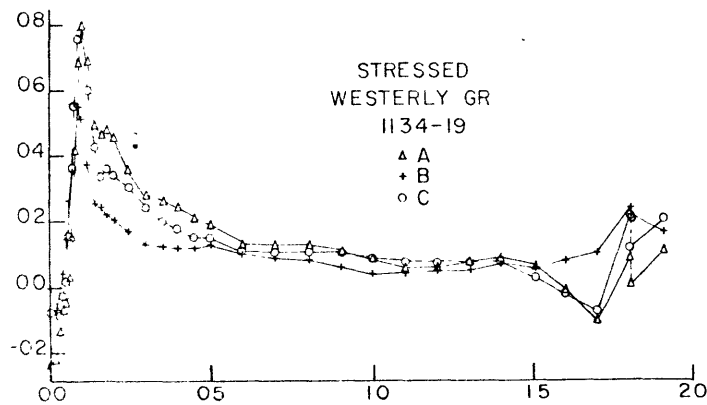
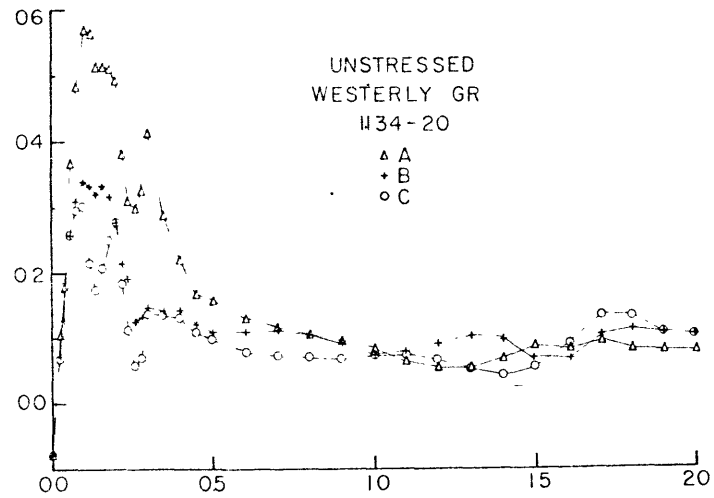


Figure 3-9. Crack closure pressure spectra in three orthogonal directions for unstressed and stressed Westerly (RI) granite. The abscissa is the closure pressure in kbars, and the ordinate is  $\nu$  in  $\text{Mbar}^{-1}$ . Many SIC have closure pressure of 100 to 200 bars and stressing increases the total crack porosity.

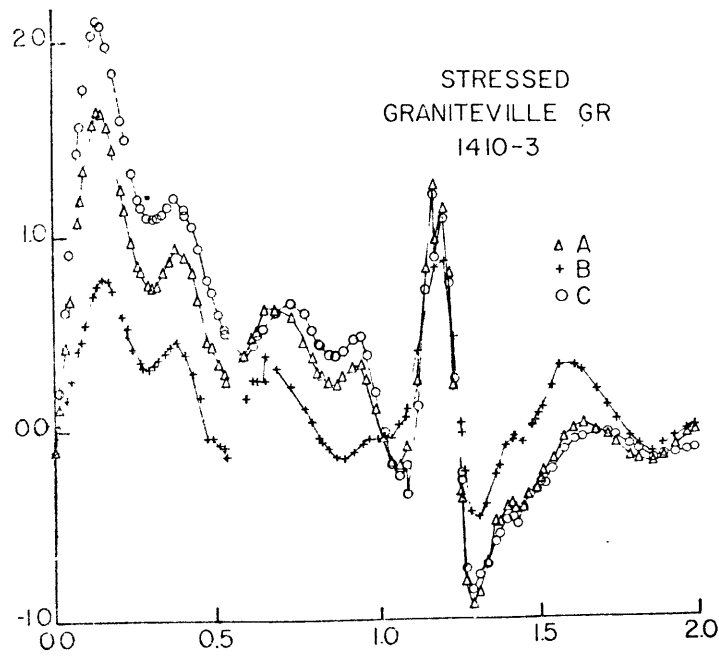
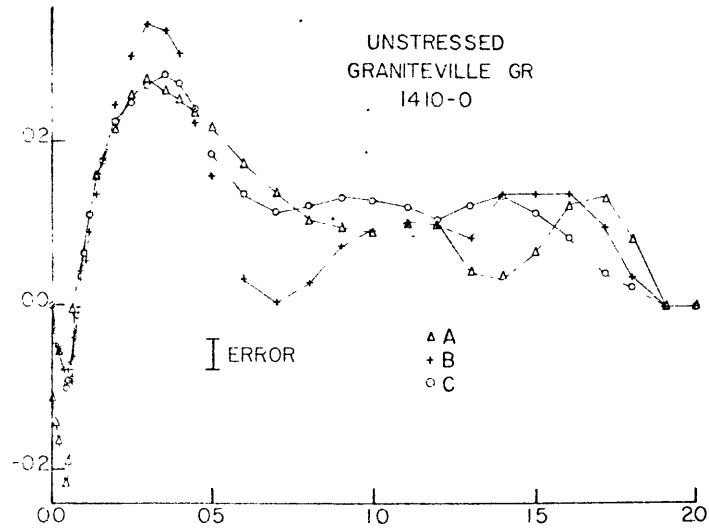


Figure 3-10. Crack closure pressure spectra in three orthogonal directions for unstressed and stressed Graniteville (MO) granite. The abscissa is the closure pressure in kbars, and the ordinate is  $v$  in  $\text{Mbar}^{-1}$ . Many SIC have closure pressure of 100 to 200 bars and stressing increases the total crack porosity.

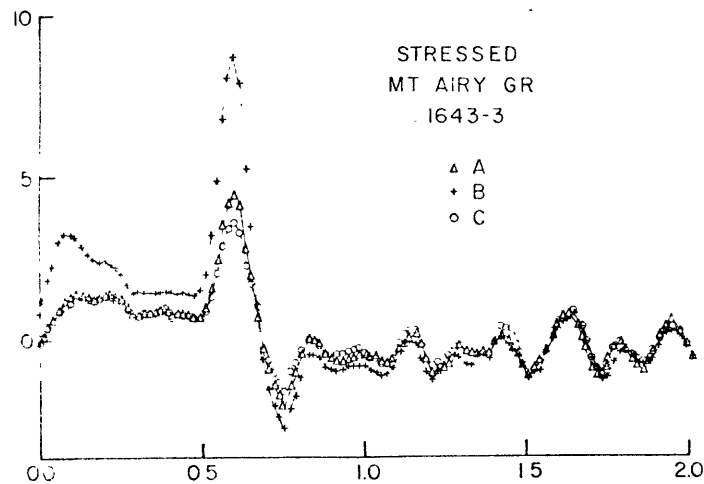
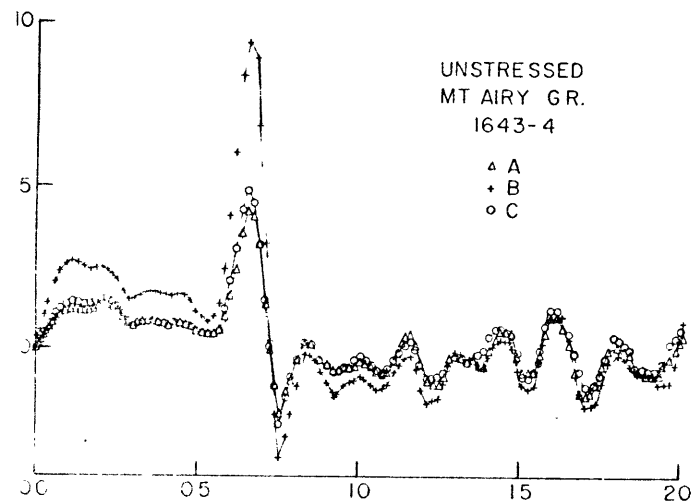


Figure 3-11. Crack closure pressure spectra in three orthogonal directions for unstressed and stressed Mt. Airy (NC) granite. The abscissa is the closure pressure in kbars, and the ordinate is  $v$  in  $\text{Mbar}^{-1}$ . Many SIC have closure pressure of 100 to 200 bars and stressing increases the total crack porosity.

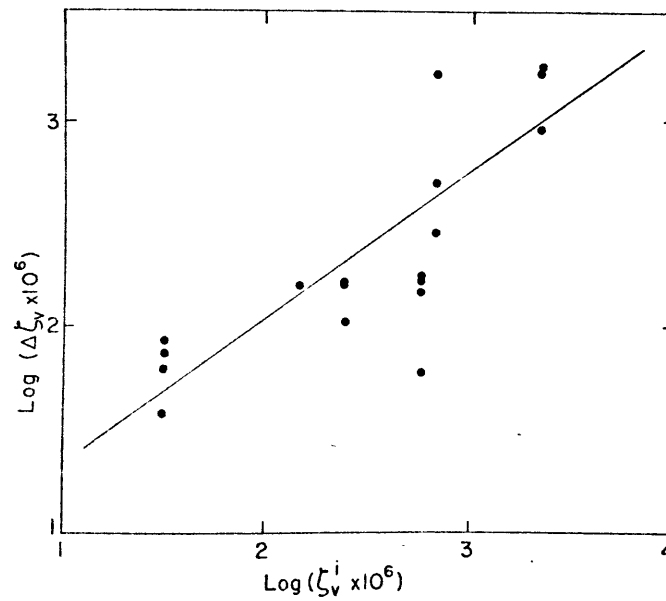


Figure 3-12. Empirical relationship between initial crack porosity and stress induced crack porosity. A least squares fit of the data is shown by the line and can be expressed as:

$$\text{Log}(\Delta\zeta \times 10^6) = 0.69\text{Log}(\zeta \times 10^6) + 0.66$$

Table 3.2

## Change in Crack Porosity due to Stressing

Sample	Maximum Load (bars)	$\zeta_v^i$ (2kb)	Log $\zeta_v^i$ (2kb)	$\zeta_v$ (2kb)	$\Delta\zeta_v$ (2kb)	Log $\Delta\zeta_v$ (2kb)
1242-15	0	32	1.51			
1242-2	3430			105	73	1.86
1242-3	3840			70	38	1.58
1242-5	3720			95	63	1.80
1242-6	3700			119	87	1.94
1331-0	0	144	2.16			
1331-4	4270			304	160	2.20
1336-0	0	242	2.38			
1336-4	2580			410	168	2.23
1336-5	2530			407	165	2.22
1336-6	2060			345	103	2.01
1134-20	0	598	2.78			
1134-8 <sup>1</sup>	1930			876	278	2.44
1134-17	1755			845	247	2.39

Table 3.2 (continued)

Sample	Maximum Load (bars)	$\zeta_V^i$ (2kb)	Log $\zeta_V^i$ (2kb)	$\zeta_V$ (2kb)	$\Delta\zeta_V$ (2kb)	Log $\Delta\zeta_V$ (2kb)
1134-18	1160			658	60	1.78
1134-19	1975			769	171	2.23
1410-0	0	685	2.84			
1410-1	2375			1188	503	2.70
1410-2	2030			980	295	2.47
1410-3	2420			1720	1035	3.01
1643-1	0	2219	3.35			
1643-2	1600			4000	1781	3.25
1643-3	1650			3174	955	2.98
1643-5	1480			4059	1840	3.26

<sup>1</sup>Sample heated to 250°C and zeta corrected for cracks introduced by heating.

ting  $\zeta_v^i$  (2kb) from  $\zeta_v$  (2kb) for each stressed sample. The scatter in the value of  $\Delta\zeta_v$  (2kb) at a particular  $\zeta_v^i$  (2kb) is due to non-identical maximum stress for each sample.

Pre-existing crack porosity also affects failure strength. A least squares fit to the data listed in Table 3.3 and plotted in Figure 3-13 shows that strength (S) is related to initial crack porosity by

$$S = 6.16 - 1.40 \text{ Log } (\zeta_v^i \times 10^6) \quad (3.2)$$

The values of S plotted in Figure 3-13 are the means for each sample of the ultimate stress listed in Table 2-3. Most samples were stressed to about 95 percent of failure strength, and the plotted strengths represent minimum values for the stress at total failure. Because the rocks examined have various mineralogies and grain sizes, we conclude that mineralogy and grain size play a subordinate role to pre-existing cracks in the formation of SIC.

### Discussion

Several aspects of the data presented in this chapter are pertinent to the evaluation of phenomena precursory to earthquakes and to the confirmation of the dilatancy-fluid diffusion model for earthquake precursors. The dilatancy-diffusion model contains assumptions about the behavior of microcracks and their effect of permeability (Scholz et al., 1973). A simplified description of the model is that

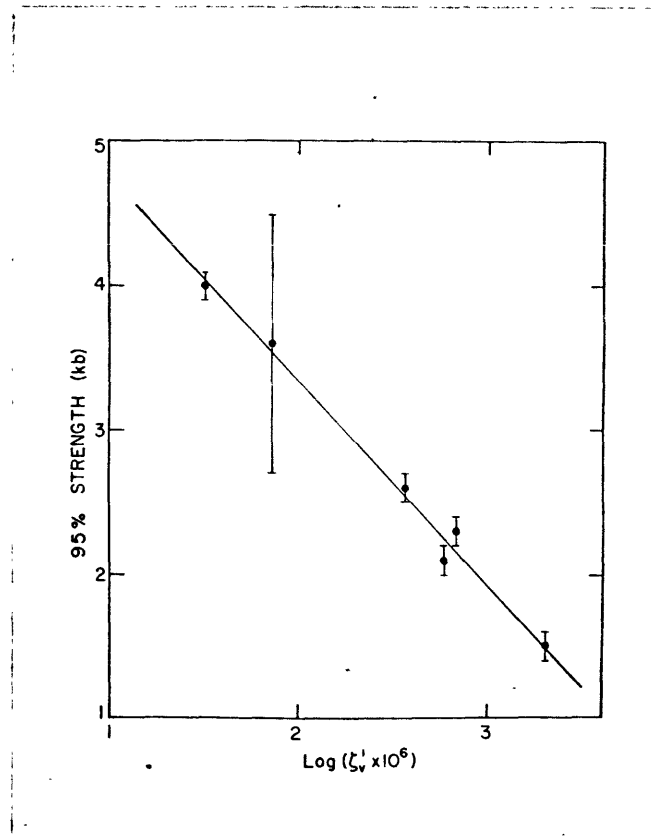


Figure 3-13. Empirical relationship between 95 percent of failure strength and initial crack porosity. A least squares fit through the data is shown by the line and can be expressed as:

$$S = 6.16 - 1.40 \text{ Log}(\zeta_v^i \times 10^6)$$



Table 3.3

## Mean Strength and Initial Crack Porosity

Sample	$10^6 \zeta_v^i$	S (kb)
1242 Frederick (MD) diabase	32	4.0 ± 0.1
1331 Mellen (WI) gabbro	73	3.6 ± 0.9
1336 Wausau (WI) granite	370	2.6 ± 0.1
1134 Westerly (RI) granite	598	2.1 ± 0.1
1410 Graniteville (MO) granite	685	2.3 ± 0.1
1643 Mt. Airy (NC) granite	2053	1.5 ± 0.1

increasing stress causes dilatant cracking. Permeability must be low enough in the initial stages of dilatant cracking to allow pore pressure to decrease. As dilatancy increases, permeability increases so that pore pressure returns to its original value. Increasing pore pressure results in catastrophic failure of the rock which is accompanied by decreasing stress. Once the stress is removed, the dilatant cracks in the rocks return to their initial 'crack-states'. The return to initial 'crack-states' means that the rock strength and measured physical properties return to their pre-stressed values.

The assumption that rocks return to their initial 'crack-states' after the stress is removed is not supported by our data which show large residual stress-induced crack porosity after the stress is removed. The observation that dilatancy is not totally recoverable at room pressure in our samples can be explained by: (1) dilatancy recovery is time dependent or (2) dilatancy is recoverable in the earth but not in the laboratory. The closure pressure of many stress-induced cracks is less than 200 bars so these cracks will be closed at depths corresponding to pressures in excess of 200 bars ( $\approx 800$  meters).

Laboratory and field studies indicate that dilatancy recovery may be time dependent. Scholz (1974) observed subsidence at a rate which decreased exponentially for one year after the 1965 Niigata, Japan earthquake ( $M = 7.5$ ).

He attributed the time dependence of dilatancy recovery to pore fluid which must outflow prior to crack closure. If Scholz's (1974) conclusion is correct that the time dependence is due to pore fluid, then dilatancy should be instantaneously recoverable in our samples which were carefully dried.

We propose that the time dependent dilatancy recovery observed by Scholz is due to a combination of inelastic crack closure and fluid flow effects. Inelastic crack closure may involve either mechanical (friction) or chemical (healing) processes. Frictional and healing processes are supported by microscopic observations in this study as well as many other studies (Richter and Simmons, 1977a; Simmons and Richter, 1976; Sprunt and Brace, 1974; Tapponier and Brace, 1976). These studies show that microcracks typically form complex networks, crack surfaces may be quite irregular and cracks are often partially or totally healed or sealed. Since in situ dilatancy recovery seems to be time dependent, rocks in tectonically active zones will become progressively weaker unless the rate of strain accumulation is slow enough to allow closing of SIC associated with previous earthquakes. By examining the rate of crack closure, we may be able to predict the periodicity of seismic events in tectonically active areas. While we do not yet know the absolute time required for closing of SIC, we predict that SIC will heal more quickly than many other types of cracks because the closure pressure of most SIC is less than the closure pressure of many other types of cracks.

Based upon Walsh's (1965) crack models, low closure pressure cracks will have lower aspect ratios (width to length ratio) than higher closure pressure cracks. A lower aspect ratio means that crack will be narrower and longer so that crack healing should occur more rapidly.

The observation that SIC form parallel sets which are oriented parallel to the direction of maximum stress indicates that the crack distribution in rocks will be strongly anisotropic in regions that are dilated by stress-induced cracks. An anisotropic crack distribution will have a profound effect on such measured physical properties as compressional and shear wave velocity, strain and permeability since cracks control the values of these properties (Brace, 1965; Brace and Orange, 1968; Birch, 1960 and 1961; Simmons, 1964; Nur and Simmons, 1969a).

Seismic waves traveling perpendicular to the plane of most SIC will have lower velocities than waves traveling parallel to most SIC. Todd et al. (1973b) have shown that linear compressibility measured parallel to the hardway direction (parallel to most cracks) in Chelmsford (MA) granite is 60 percent less than compressibility measured parallel to the rift direction (normal to most cracks) and compressional and shear wave velocity in the hardway direction is about 55 percent greater than the velocity in the rift direction. Therefore, unless the azimuthal distribution of seismic sources and receivers is considered with respect to

the stress state and crack distribution, the observed decrease and subsequent increase of velocity in focal regions prior to large earthquakes may be due to differences in the ray paths of seismic waves and not to changes in the rock properties. Consider the sequence of events shown in Figure 3-14. The seismic waves from event 1 have velocities  $P_1$  and  $S_1$  and traverse the dilatant zone such that the ray path is not normal to most cracks. The ray paths of seismic waves from event 2 are normal to most cracks so that the measured velocities  $P_2$  and  $S_2$  will be less than  $P_1$  and  $S_1$ . Event 3 produces seismic waves with ray paths and velocities identical to those of event 1. The decrease then increase in velocity observed at station A is due solely to differences in ray paths for different events and not to changes in the properties of the rock.

While crack anisotropy complicates measurements of compressional and shear wave velocity ratios, it provides us with a new tool for predicting earthquakes. Nur and Simmons (1969b) and Todd et al. (1973b) have shown experimentally and Nur (1971) has shown theoretically that an anisotropic distribution of cracks produces splitting of shear waves into two components which travel with different velocities. The velocity difference increases with increasing anisotropy. By monitoring the difference in travel times between the two S-waves, we should be able to determine changes in the 'crack-states' of rocks prior to earthquakes. Gupta (1973a and b) has

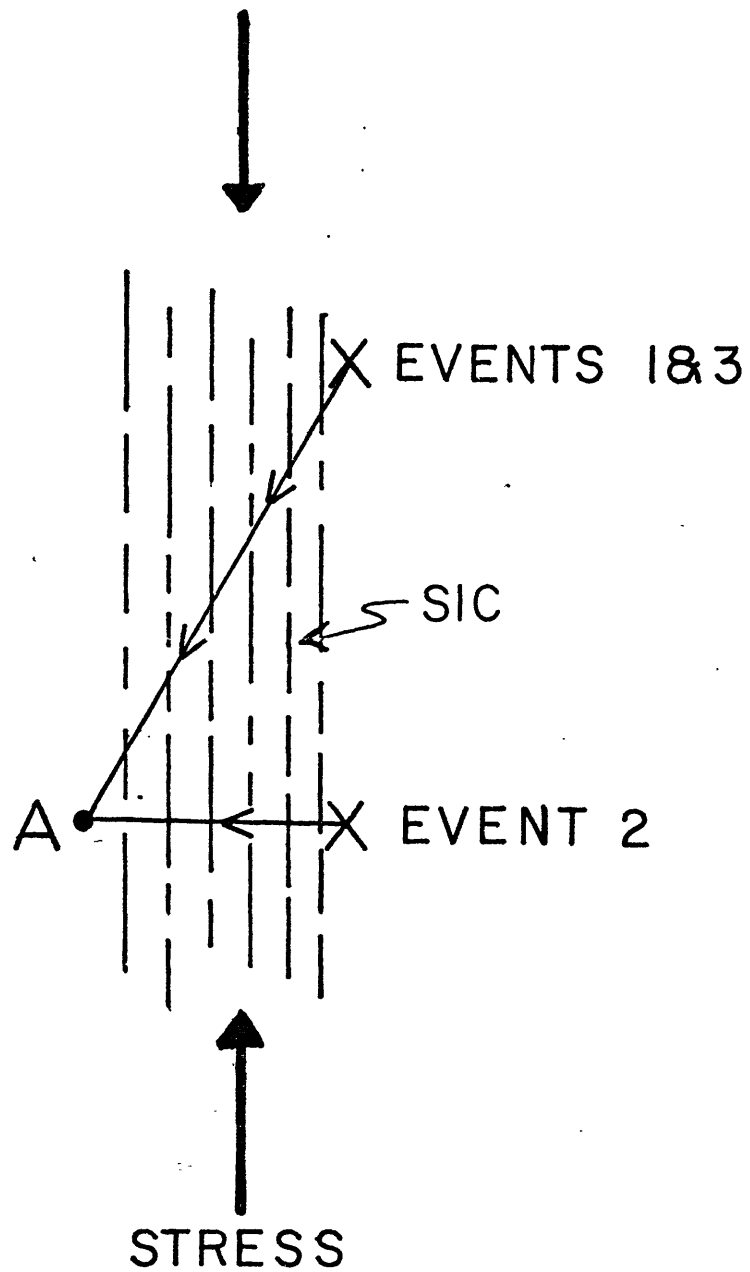


Figure 3-14. Relationship between seismic ray paths and crack orientation. Seismic waves from event 2 will have lower velocity than waves from events 1 and 3.

monitored shear wave splitting prior to earthquakes in Nevada and he has shown that earthquakes are preceded by increases in the difference between the travel times of the two shear waves. He concluded that the physical properties of rocks in focal regions become increasingly anisotropic due to increased microcrack dilatancy prior to earthquakes.

Crack anisotropy will also affect diffusion of fluids into and out of dilated regions. SEM observations indicate that SIC are not generally interconnected, but the SEM affords only a two dimensional view. Results from DSA and three dimensional observations with the petrographic microscope show that many SIC are interconnected via pre-existing cracks and stressing reopens partially healed cracks. Therefore, we predict large increases in permeability parallel to the direction of maximum stress and slight increases perpendicular to the maximum stress axis. We have not yet measured permeability nor can we yet determine the magnitude of the permeability increase from crack characteristics. Zoback and Byerlee (1975b) measured permeability as a function of triaxial stress in Westerly (RI) granite and found that increasing dilatancy caused increased permeability in the direction of maximum compression, but the increase was insufficient to explain fluid flow rates in the field. We suggest that end loading conditions 'clamped' their samples (see Chapter 2).

CHAPTER 4  
EFFECTS OF HYDROSTATIC PRESSURE CYCLING AND UNIAXIAL  
STRESS CYCLING

Introduction

A requirement of current models for earthquake precursors is that rocks dilate prior to earthquakes (Scholz et al., 1973; Mjachkin et al., 1975). One major problem associated with these models is that dilatancy in laboratory samples requires shear stresses which are considerably higher than in situ stresses inferred from heat flow data (Brune et al., 1969; Henyey and Wasserberg, 1971; Lachenbruch and Sass, 1973) or from direct measurements of in situ stress (Hast, 1969; Hooker and Johnson, 1969; Kropotkin, 1972). Recently, Scholz and Kranz (1974), Haimson (1974), Zoback and Byerlee (1975a), and Hadley (1976) have shown that in uniaxial and low confining pressure (<1.5kb) triaxial experiments, the onset of dilatancy occurs at progressively lower stress in rocks subjected to cyclic loading. Cyclic fatigue might explain why laboratory measurements of shear stress at the onset of dilatancy are higher than measurements of in situ stress in areas of repeated seismic activity. However, Zoback and Byerlee (1975a) and Hadley (1976) did not observe cyclic fatigue in rocks subjected to confining pressure greater than 2 kbar. The cyclic fatigue mechanism can only be invoked for earthquakes shallower than about 10 km.



In this chapter, we examine the effects of uniaxial stress cycling and hydrostatic pressure cycling on microcracks in rocks. The purpose of our experiments is to gain a detailed understanding of how rocks fail under cyclic loading. Our results are also useful to experimenters who attempt to duplicate in situ conditions by placing rocks under various stress states.

#### DSA Results

Cracks in several granites have been examined with DSA over two or three hydrostatic pressure cycles. In general, we find that there is a 20 to 50 percent decrease in total crack porosity between the first and second pressure cycles, but less than a 30 percent decrease between the second and third cycles. The decrease in porosity between cycles can be related to unrecovered strain when the pressure is removed. We attribute this inelastic behavior to cracks which do not reopen.

The zero pressure crack porosity,  $\zeta$ , and unrecovered strain for several samples are listed in Table 4.1. The unrecovered strain is defined as the strain at zero pressure after the rock is subjected to hydrostatic pressure, minus the strain at zero pressure before the pressure cycle. We use the convention that compressive strains are negative. Some strain gages show a positive unrecovered strain which is due to stretching of the strain gage when the gage is mounted

Table 4.1

Changes in  $\zeta(P)$  due to Hydrostatic Pressure Cycling<sup>1</sup>

Sample	Direction	$\zeta(P) \times 10^{62}$			$\Delta\zeta(P) \times 10^6$		$\frac{\Delta\zeta}{\zeta} \times 100$		Unrecovered Strain	
		Cycle 1	Cycle 2	Cycle 3	Cycle 1 to 2	Cycle 2 to 3	Cycle 1 to 2	Cycle 2 to 3	After Cycle 1	After Cycle 2
1374-1	A	70	56	50	-14	-6	-20	-11	-24	-9
	B	95	67	65	-28	-2	-30	-3	-56	-12
	C	180	104	85	-76	-19	-42	-18	-83	-6
	Total	345	227	200	-118	-27	-34	-12	-163	-27
1374-2	A	96	47	40	-49	-7	-51	-15	-43	-2
	B	115	70	53	-45	-17	-39	-24	-51	4
	C	170	79	67	-91	-12	-54	-15	-55	18
	Total	381	196	160	-185	-36	-49	-18	-149	20
1134-1 <sup>3</sup>	A	712	464		-248		-46		-155	
	B	547	365		-182		-33		-222	
	C	518	280		-238		-36		-221	
	Total	1777	1109		-668		-38		-598	
1134-7 <sup>3</sup>	B	670	408	348	-262	-60	-39	-15	-204	-8

Table 4.1 (continued)

Sample	Direction	$\zeta(P) \times 10^{62}$			$\Delta\zeta(P) \times 10^6$		$\frac{\Delta\zeta}{\zeta} \times 100$		Unrecovered Strain	
		Cycle 1	Cycle 2	Cycle 3	Cycle 1 to 2	Cycle 2 to 3	Cycle 1 to 2	Cycle 2 to 3	After Cycle 1	After Cycle 2
1134-8 <sup>3</sup>	A	883	572	525	-311	-47	-35	-8	-205	34
	C	658	386	348	-272	-38	-41	-10	-238	-17
	Total <sup>4</sup>	2199	1344	1221	-855	123	-39	-9	-681	0
1134-13 <sup>3</sup>	A	795	400	340	-395	-60	-50	-15	-200	2
1134-15 <sup>3</sup>	A	687	264	260	-423	-4	-62	-2	-38	36
	C	601	262	183	-339	-79	-56	-30	-224	58
	Total <sup>4</sup>	1889	788	626	-1101	-162	-58	-20	-486	152
1134-16 <sup>3</sup>	A	410	296		-114		-28		-123	
	B	322	240		-82		-25		-80	
	C	273	198		-75		-27		-126	
	Total	1005	734		-271		-27		-329	
1134-17	A	351	275		-76		-22		-22	
	B	247	220		-27		-11		33	
	C									

Table 4.1 (continued)

Sample	Direction	$\zeta(P) \times 10^{62}$			$\Delta\zeta(P) \times 10^6$		$\frac{\Delta\zeta}{\zeta} \times 100$		Unrecovered Strain	
		Cycle 1	Cycle 2	Cycle 3	Cycle 1 to 2	Cycle 2 to 3	Cycle 1 to 2	Cycle 2 to 3	After Cycle 1	After Cycle 2
1134-17	Total <sup>4</sup>	845 <sup>4</sup>	715		-130		-15		44	
1134-18	A	276	267		-9		-3		61	
	B	191	190		-1		0		-37	
	Total <sup>4</sup>	658 <sup>4</sup>	547		-11		-2		-3	
1134-19	A	276	239		-37		-13		-3	
	B	205	184		-21		-10		35	
	C	288	110		-178		-62		-34	
	Total	769	533		-236		-31		-2	
A757-1	A	1038	445	235	-593	-210	-57	-47	-325	23
	B	432	206	110	-226	-96	-52	-47	-159	-6
	C	338	320	262	-18	-58	-5	-27	-324	8
	Total	1808	971	607	-837	-364	-46	-37	-808	25

<sup>1</sup>Total  $\zeta(P)$  is the zero pressure crack porosity,  $\zeta_v(P)$ , for cracks which close by pressure P.

<sup>2</sup>P = 1 kbar for all cycles except cycles 1 and 2 of sample 1134 where P = 2 kbar. Most cracks are closed by 1 kbar so  $\zeta(1kb) \approx \zeta(2kb)$ .

Table 4.1 (continued)

---

<sup>3</sup>Sample heated to 250°C and no correction is made for thermally induced cracks.

<sup>4</sup>Total obtained by combining zeta in the A (rift) direction with twice zeta in the B (grain) or C (hardway) directions.

over a large crack or air bubble in the epoxy.

The Westerly (RI) granite samples (#1134) were pressure cycled twice to 2 kbars and  $\zeta(2\text{kb})$  tabulated. Some Westerly granite samples were cycled a third time to 1(kb), and  $\zeta(1\text{kb})$  is tabulated. All other samples were pressure cycled to 1 kbar, 2 kbars, then 4 kbars. In order to compare the data for successive pressure cycles we have tabulated  $\zeta(1\text{kb})$  for these samples. From analysis of crack closure pressure spectra we find that most cracks are closed by 1 kbar so that  $\zeta(1\text{kb})$  is approximately equal to zeta for higher pressures.

In this study, we also examined briefly the effect of uniaxially restressing samples that had been hydrostatically pressure cycled. After one stress cycle to 90 percent of failure and two pressure cycles to 2 kbars, samples 1134-17, 1134-18, and 1134-19 were restressed to loads which were 25 to 175 bars less than the original stress. Figure 4-1 shows typical closure pressure spectra in the A direction for a restressed sample. The shape of the spectrum after restressing approximates the original closure pressure spectrum and the area under curve 3 is larger than under curve 1. The increase in area indicates that restressing increases the crack porosity. These data show that uniaxially stressing a sample reopens cracks which were 'permanently' closed by hydrostatic pressure and produces new SIC.

The effects of stress cycling were examined further by uniaxially stressing samples of Westerly (RI) granite and

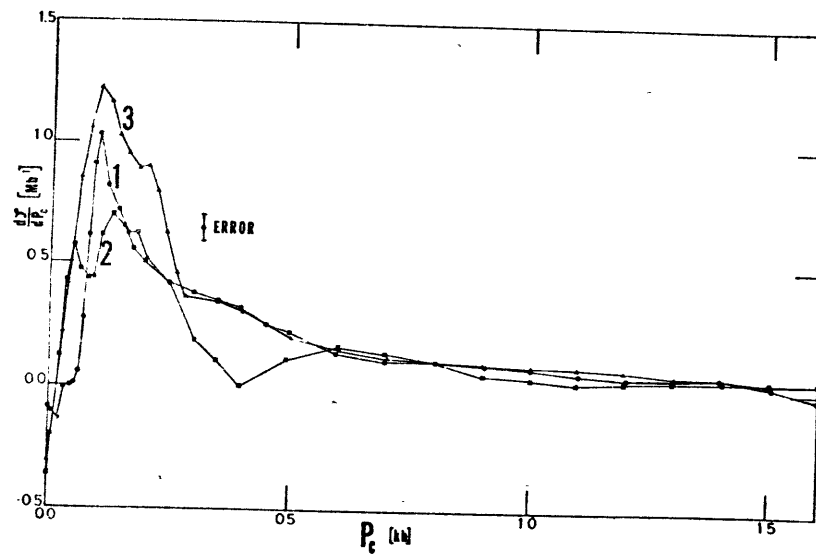


Figure 4-1. Closure pressure spectra in the direction of maximum strain for stressed sample 1134-17. Numbers refer to cycle number. Data for cycles 1 and 2 were taken after initial stressing and show the effects of hydrostatic pressure cycling. Third-cycle data were taken after restressing to 100 bars less than the original stress. After restressing, the shape of the spectrum approximates the original spectrum. The error for data below 300 bars is indicated by the error bar. Error is reduced at higher  $P_c$ .

Frederick (MD) diabase. Each Westerly granite sample was stressed three times to about 90 percent of failure. The effects of stress were examined with DSA after each stress cycle. For these samples we observe a 7 to 30 percent increase in crack porosity after the second stressing, and a 20 to 40 percent increase between the first and third stress cycles. The largest increase in zeta was in the rift direction, with almost no change in zeta in the grain direction. This observation is consistent with the previous data that most SIC are formed in the rift plane which was parallel to the direction of maximum stress (Feves and Simmons, 1976). Sample 1134-18 was stressed to a value equal to the load required for the onset of dilatancy,  $C'$  (Brace et al., 1966). No change in crack porosity for sample 1134-18 was observed after the second stressing, but an 8 percent increase was found after the third stressing. Maximum loads for each stress cycle and numerical values of  $\zeta(2kb)$  for the Westerly stress cycled samples are shown in Table 4.2.

Each Frederick diabase sample was stressed several times prior to analysis with DSA. The number of stress cycles, maximum stress, and DSA results are listed in Table 4.3. These data show little or no increase in crack porosity even after seven stress cycles. We will discuss these Westerly granite and Frederick diabase results in the next section.



Table 4.2

 $\zeta(2kb)$  for Stress-Cycled Westerly Granite

Sample No.	Direction	First Stressing		Second Stressing			Third Stressing		
		Load	$\zeta(2kb) \times 10^6$	Load	$\zeta(2kb) \times 10^6$	$\Delta(\%)^1$	Load	$\zeta(2kb) \times 10^6$	$\Delta(\%)^1$
1134-17	A	1755	351	1670	428	+22	1645	521	+48
	B		247		224	-9		219	-11
	C				255			287	
	Total		845 <sup>2</sup>		907	+7		1027	+22
1134-18	A	1160	276	1140	285	+3	1130	312	+13
	B		191		222	+16		222	+16
	C				148			187	
	Total		658 <sup>2</sup>		655	0		721	+10
1134-19	A	1975	276	1800	499	+81	1775	527	+91
	B		205		212	+3		222	+8
	C		288		305	+6		353	+23
	Total		769		1016	+32		1102	+43

<sup>1</sup>Percentage of change referred to first cycle data.

<sup>2</sup>Total obtained by combining  $\zeta(2kb)$  in the rift direction (A) with twice  $\zeta(2kb)$  in the grain or or hardway directions (B or C).

Table 4.3

 $\zeta$ (2kb) for Stress-Cycled Frederick Diabase

Sample No.	Direction	$\zeta$ (2kb) $\times 10^6$	Maximum Stress (bars)						
			Cycle 1	Cycle 2	Cycle 3	Cycle 4	Cycle 5	Cycle 6	Cycle 7
1242-15	A	0	0						
	B	10							
	C	22							
	Total	32							
1242-2	A	30	3430						
	B	45							
	C	0							
	Total	105							
1242-3	A	40	3840						
	B	0							
	C	30							
	Total	70							
1242-5	A	0	3720						
	B	95							

Table 4.3 (continued)

Sample No.	Direction	$\zeta(2kb) \times 10^6$	Maximum Stress (bars)						
			Cycle 1	Cycle 2	Cycle 3	Cycle 4	Cycle 5	Cycle 6	Cycle 7
1242-5	C	0							
	Total	95							
1242-6	A	60	3700						
	B	9							
	C	50							
	Total	119							
1242-14	A	15	3970	2310					
	B	5							
	C	5							
	Total	25							
1242-12	A	13	3150	3140	3140	3160			
	B	13							
	C	5							
	Total	31							
1242-11	A	14	3490	3180	2940	3450	3350	3390	3020

Table 4.3 (continued)

Sample No.	Direction	$\zeta(2kb) \times 10^6$	Maximum Stress (bars)						
			Cycle 1	Cycle 2	Cycle 3	Cycle 4	Cycle 5	Cycle 6	Cycle 7
1242-11	B	26							
	C	0							
	Total	40							

## Discussion

Our DSA data from hydrostatically pressure cycled samples indicate that many cracks closed by hydrostatic pressure do not reopen after the pressure is removed. This behavior can be attributed to friction along crack surfaces which hold cracks closed or to the crushing of bridges which propped cracks open. Bridges formed in cracks which are in equilibrium with the applied stresses do not prop cracks open, but if the stress state in the vicinity of a crack changes after formation of the bridges, then the bridges may in effect, prop the crack open. If application of hydrostatic pressure crushes these bridges the cracks will not reopen. Partially healed crack contain bridges, but we have not yet microscopically examined samples which have been hydrostatically pressure cycled to determine if crushed material is present in partially healed cracks. The frictional mechanism is supported by our observations with the SEM and PM that cracks often form complex networks and have irregular surfaces.

The observations that some crack in hydrostatically pressure cycled samples do not reopen after the pressure is removed is pertinent to virtually all experiments which attempt to duplicate in situ conditions by placing samples under simulated in situ pressure and temperature conditions in the the laboratory. These experiments may not be valid analogues because they do not duplicate in situ crack characteristics, and the interpretation of data obtained in such analogue experiments

may be incorrect because cracks control the values of many physical properties.

A solution to the problem of determining in situ physical properties from direct laboratory measurements is to base physical properties determinations on crack characteristics rather than try to measure physical properties directly. For example, Feves et al. (1977) measured electrical resistivity on a suite of Frederick (MD) diabase samples which differed only in crack porosity to obtain:

$$\text{Log } \rho = 11.97 - 3.11 \text{ Log } (\eta_v(0) \times 10^6)$$

where  $\rho$  is electrical resistivity in ohm-meters and  $\eta_v(0)$  is the crack porosity at zero confining pressure. They deduced in situ crack porosity as a function of depth from DSA data to determine electrical resistivity versus depth. By using crack characteristics rather than direct measurements of electrical resistivity, they eliminated the effects of conduction along crack surfaces which is present in laboratory experiments but may not be present in situ.

Another problem with high pressure laboratory studies is the common practice of placing copper jackets around samples to prevent leakage of the pressure medium into the sample (Brace, 1964 and 1965). The jacketed samples are then subjected to one or two kilobars of hydrostatic pressure to 'seat' the copper jacket uniformly against the rock surface. Our data show that this 'seating' process may alter the microstructure of the rock. Therefore, the interpretation of measurements

made subsequent to jacket seating may be erroneous unless changes in the crack characteristics are considered. One way of avoiding this problem is to use elastomer encapsulents rather than copper jackets.

The results from our uniaxial stress cycling experiments support the observation in Chapter 3 that pre-existing cracks enhance the production of SIC. The initial crack porosity of Westerly granite is  $598 \times 10^{-4}$  percent and crack porosity increases with each stress cycle. An explanation for this behavior is that SIC formed by previous stressing provide sites of stress concentration for subsequent stressings. Frederick diabase contains very few cracks ( $\zeta_v < 30 \times 10^{-6}$ ) to provide stress concentration sites so we should not expect to induce many new cracks by stressing. In fact, we observe very few SIC in Frederick diabase, even after seven stress cycles to 95 percent of failure.

An alternative explanation for the behavior of Frederick diabase is based upon the fact that it is primarily composed of fine grained plagioclase and augite and contains no quartz. Nur and Simmons (1970) attribute cracking in rocks to the presence of quartz because the thermal and mechanical properties of quartz are quite different from other silicate minerals. The compressibilities of plagioclase and augite are quite similar so there should be very little mismatch in elastic properties between mineral grains in the Frederick diabase, and we should expect very little cracking.

One implication from the results of these stress cycling experiments and from the data in Figures 3-12 and 3-13 is that rocks in tectonically active zones will become weaker with time unless stress induced cracks heal between successive earthquakes. By examining healed SIC in rocks from fault zones we may be able to determine earthquake history and predict earthquake periodicity.



## CHAPTER 5

## ANALYSIS OF SIC IN A GRANITE CORE

Introduction

In this chapter the results and techniques developed for our characterization of laboratory SIC are applied to the analysis of the cracks in a 1.5 km core from Shannon County in southeastern Missouri. The core is designated Sh-13 by Kisvarsanyi (1975) and we shall maintain this designation with the addition of a number corresponding to the depth in meters of a particular sample. This core was chosen because it is primarily granite which has constant mineralogy and grain size along most of its length. The granite is intruded by aplite and diabase dikes, but these dikes were avoided during selection of core samples. The consistency of the composition of the granite was verified by point counting, and Table 5.1 presents the modal analysis for several samples. A description of the core as a function of depth can be found in Appendix I.

This core is also interesting because it comes from an intraplate region which is tectonically unstable and geologically complex. While no orogenic processes have taken place since the Precambrian, there is considerable crustal instability in the area. Many seismologists consider the New Madrid, Missouri earthquake of 1812 as one of the largest earthquakes in North America (Fuller, 1912). The geologic

Table 5.1

## Modal Analysis of Sh-13 as a Function of Depth

Depth = Mineral	609		763		1056		1316		1523	
	Grain Size (mm)	Volume Percent	Grain Size (mm)	Volume Percent	Grain Size (mm)	Volume Percent	Grain Size (mm)	Volume Percent	Grain Size (mm)	Volume Percent
Quartz	0.5-1.5	29.1	0.5-2.0	26.8	0.3-2.0	35.9	1.5-4.0	19.5	0.5-4.0	26.8
Plagioclase	0.5-1.0	0.7	1.0-2.0	9.6	0.8	4.3	0.5-5.0	17.0	0.5-5.0	14.7
K-Feldspar	0.5-1.5	4.1	2.0	8.7	1.0-1.5	4.0	1.0-1.5	7.2	0.5-1.0	3.1
Perthite	1.0-4.0	54.8	1.5-4.0	42.4	1.0-2.0	40.7	1.5-5.0	46.5	2.0-6.0	47.3
Microcline	1.0	1.7	0.5-1.0	1.0	1.0	1.5	2.0	0.9	3.0-6.0	2.0
Biotite	0.5-1.5	5.1	0.3-0.5	6.2	0.1-0.3	5.1	0.1-1.0	1.8	<1.0	2.1
Chlorite	0.5	0.5	0.3-0.5	0.8	0.1-0.3	1.4	0.1-1.0	1.5	<0.7	1.6
Epidote	<0.1	1.4	0.5	0.3	<0.1	1.0	<0.1	3.1	<0.1	0.4
Allanite	0.2	0.7	0.5	1.2	0.1-0.3	1.5	0.1-2.0	0.2		tr
Fluorite			1.5	0.8	0.2-0.7	1.3			<0.3	0.2
Apatite			0.3	0.4	<0.1	1.6	<0.1	1.1		
Zircon	0.1-0.5	1.1	0.3	0.5	0.1-0.2	0.9	0.1-0.3	1.0	0.1	0.2
Opauques			0.3	tr			0.3	0.2	<0.1	0.2

Table 5.1 (continued)

Depth =	609		763		1056		1316		1523	
Mineral	Grain Size (mm)	Volume Percent	Grain Size (mm)	Volume Percent	Grain Size (mm)	Volume Percent	Grain Size (mm)	Volume Percent	Grain Size (mm)	Volume Percent
Others	0.5-1.0	0.9 <sup>1</sup>		1.2 <sup>2</sup>		0.8 <sup>3</sup>			0.5-1.0	1.3 <sup>4</sup>
Total		100.1		99.9		100.0		100.0		99.9
Number of counts		1001		1000		1000		1000		1000

<sup>1</sup>Amphibole.

<sup>2</sup>Altered feldspar (epidote?).

<sup>3</sup>Carbonate and trace of muscovite.

<sup>4</sup>Carbonate.

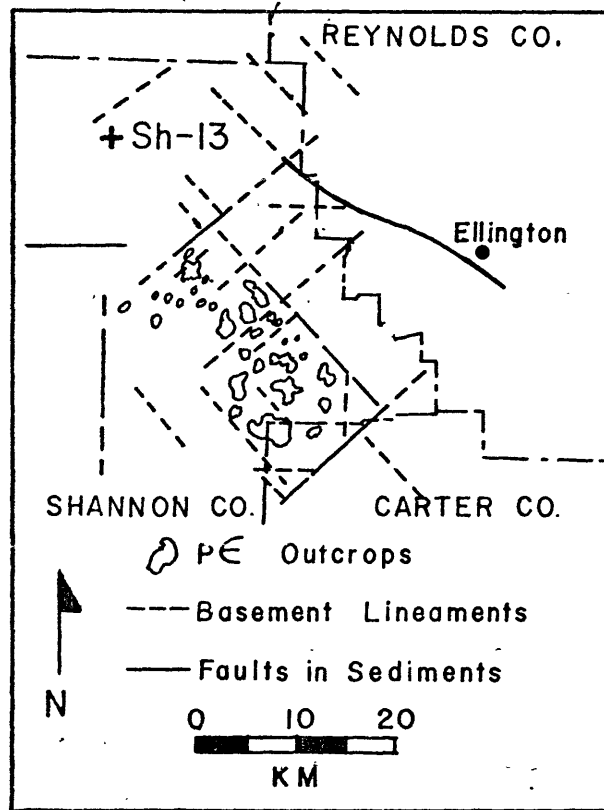


Figure 5-1. Location of the Sh-13 core. Lineaments, faults and geology are adopted from Kisvarsanyi (1976).

history of the area has been thoroughly studied (Berry and Bickford, 1973; Bickford and Mose, 1975; Kisvarsanyi, 1974; Kisvarsanyi and Kisvarsanyi, 1976). Kisvarsanyi and Kisvarsanyi (1976) used structural geology, airphotos, aeromagnetic maps and ERTS-1 imagery to determine the major structural lineaments in the Precambrian basement. The location of the Sh-13 core with respect to these lineaments is shown in Figure 5-1.

#### DSA Results

We performed differential strain analysis on 12 samples from depths of 400 to 1500 meters. Crack porosity at zero confining pressure due to cracks which close between zero and 2 kbars,  $\zeta_v$  (2kb), is represented by open circles in Figure 5-2 and is tabulated in Table 5.2. However,  $\zeta_v$  (2kb) does not represent the in situ crack porosity since pressure at depth is probably non-zero. Zero pressure crack porosity is the upper limit for in situ crack porosity. If we assume lithostatic pressure with depth and zero pore pressure, then we obtain a lower limit for in situ crack porosity,  $\zeta_v^D$  (2kb), as shown by the closed circles in Figure 5-2. Thus, we can determine upper and lower bounds for the in situ crack porosity.

Normally, crack porosity should decrease monotonically with depth as shown by the porosity profile in Figure 5-2 for depths less than 1 km, but the data in Figure 5-2 shows an

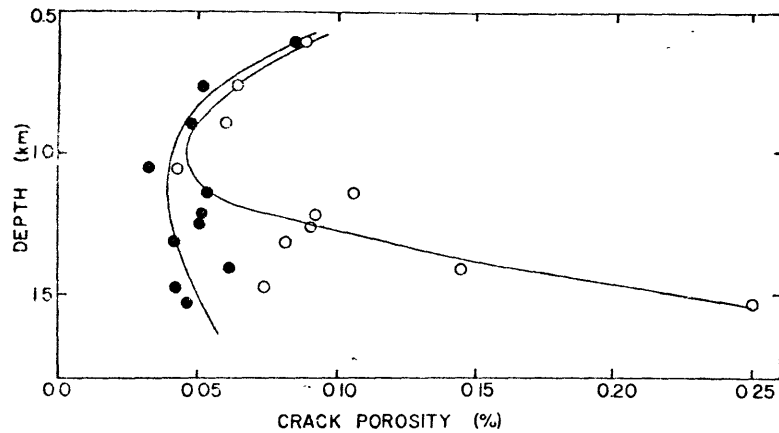


Figure 5-2. Crack porosity versus depth in the granite core from Shannon County, Missouri (Sh-13). The open circles are the zero pressure crack porosity (upper limit) and the closed circles represent the porosity profile if lithostatic pressure with depth and zero pore pressure is assumed (lower limit). Non-decreasing crack porosity below 1 km indicates the presence of directed stress.

Table 5.2

Crack Porosity as a Function of Depth for Sh-13

Depth	Pressure <sup>1</sup>	$\zeta_V$ (2kb)	$\zeta_V^D$ (2kb)
609m	160b	888	850
763	200	639	516
899	235	600	471
1056	276	429	322
1140	298	1056	535
1219	318	917	512
1257	329	909	506
1316	345	815	413
1410	369	1442	612
1473	385	738	420
1523	399	2492	460

<sup>1</sup>In situ lithostatic pressure assuming zero pore pressure and average rock density of 2.67 gm/cm<sup>3</sup>.

increase or at least constant porosity with increasing depth below about 1 km. We attribute the increase in porosity below 1 km to changes in the stress state from lithostatic or hydrostatic above 1 km to non-lithostatic below 1 km.

Further evidence for tectonic stress below 1 km can be seen in the crack spectra. Typical crack closure pressure spectra in the direction of maximum principal strain are shown in Figure 5-3. These spectra show the strain associated with cracks at each closure pressure,  $P_c$ . The left two spectra are representative of spectra for samples shallower than 1 km. These spectra consist of a single broad peak with most cracks closed above 1 kbar. Spectra for samples from below 1 km show an increase in the amplitude of the broad peak which indicates an increase in porosity with depth. We also observe development of a second peak at about 150 bars superimposed upon the broad peak. The superimposed peak first appears at 1140 meters and becomes more pronounced with depth. Based upon our laboratory studies which showed that closure pressures of 100 to 200 bars are characteristic of stress-induced cracks, we conclude that the peak at 150 bars is due to the presence of SIC. However, these SIC are not open in situ because the confining pressure below 1 km is probably greater than 150 bars.



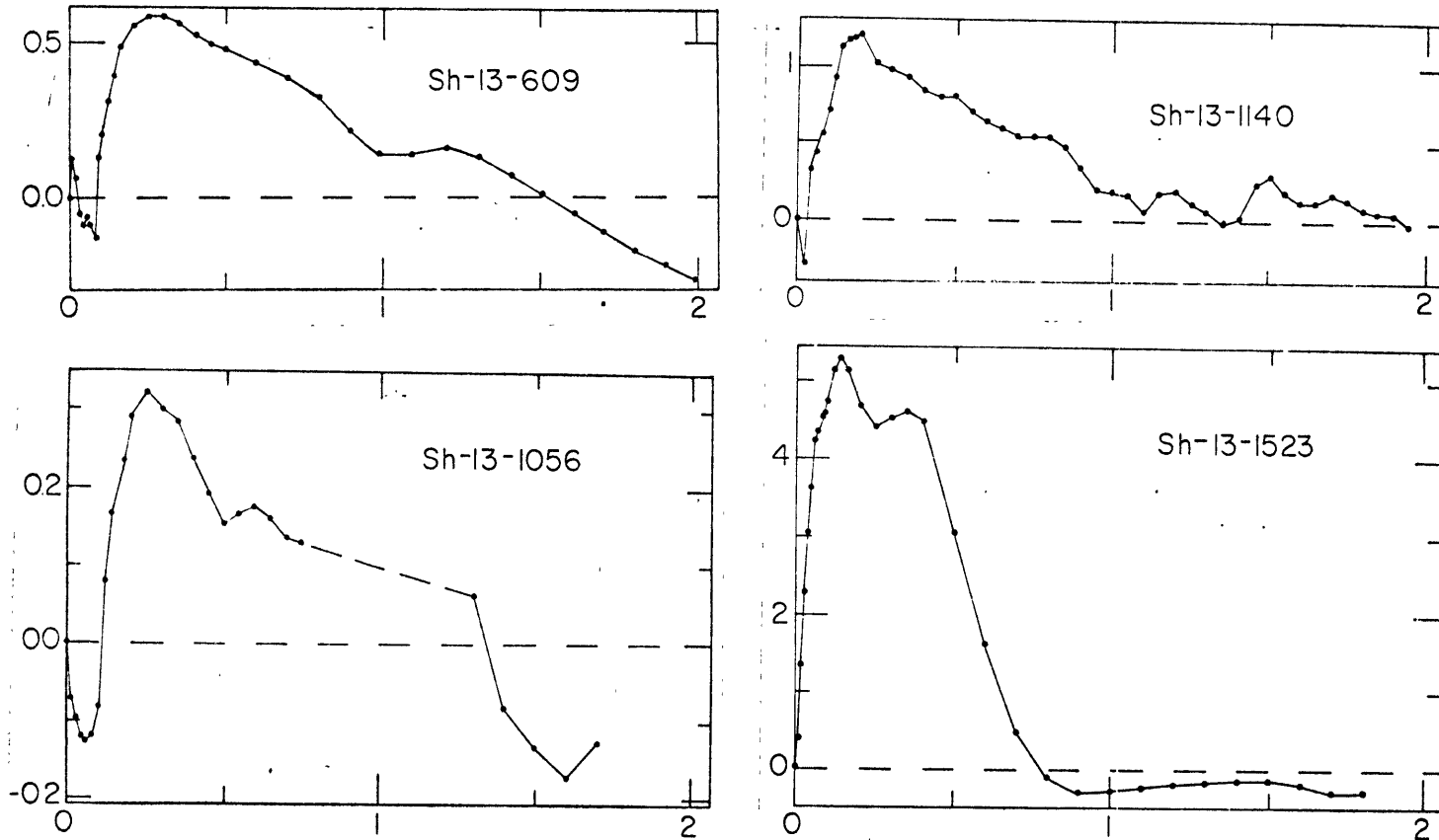


Figure 5-3. Typical crack closure pressure spectra for Sh-13 in the direction of maximum principal strain. The development of a pronounced peak at 150 bars below 1 km indicates the presence of SIC below 1 km. The abscissa is the closure pressure in kbars, and the ordinate is  $\nu$  in  $\text{Mbar}^{-1}$ .

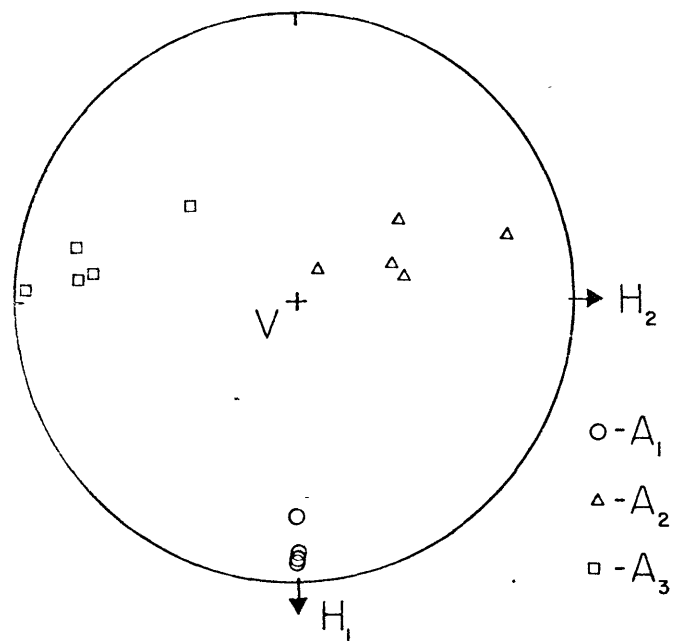


Figure 5-4. Stereographic projection of the poles to the crack planes for 150 bar cracks in Sh-13 below 1 km. All SIC are aligned at less than 20 degrees from vertical.

With DSA we can also determine the orientation of the 150 bar stress-induced cracks. Figure 5-4 is a stereographic projection of the orientation of the principal axes of zeta at closure pressure of 150 bars for samples from depths greater than 1 km. The greatest, intermediate, and least principal axes are denoted by  $A_1$ ,  $A_2$ , and  $A_3$ , respectively. The projection is on the lower hemisphere with the core axis vertical. The horizontal axes,  $H_1$  and  $H_2$ , are arbitrary with respect to field orientation of the core since in situ core orientation is unknown. We have rotated the reference axes of each core sample to gain greatest alignment of the maximum principal strain,  $A_1$ . Figure 5-4 shows that in all cases the maximum principal strain axis is tilted at less than 20 degrees from horizontal. Therefore, the set of 150 bar cracks is tilted at less than 20 degrees from vertical.

The consistency of these DSA data indicate that the 150 bar cracks are a result of processes acting upon the rock in situ. These cracks were not introduced as a direct result of drilling or sample preparation.

### Microscopic Observations

In Chapter 3 we showed that many SIC are transgranular, they may cross many grain boundaries, form parallel to sub-parallel sets, and are planar. In this section, we shall show that many cracks in the Sh-13 core from below 1 km have characteristics indicative of stress-induced cracks.

Figure 5-5 is a photo mosaic made with the SEM for sample Sh-13-1523. This mosaic contains examples of cracks which meet all of the criteria for SIC. The cracks marked SIC are transgranular, they cross several grain boundaries, and form a parallel set. The orientation of these SIC at 15 degrees from vertical agrees with the DSA results. SIC are particularly abundant in this section from 1523 meters, but they can also be found in all samples from below 1 km.

Figure 5-6 is an SEM mosaic of a crack section from sample Sh-13-1056. The transgranular crack which crosses the quartz-feldspar grain boundary is a SIC. Note that the SIC in Figures 5-5 and 5-6 were formed recently since no evidence of healing is present. The cracks have sharp terminations and no bridging material. We will return to this point when we discuss mechanisms of crack formation in the next section.

When we examine thin sections and crack sections from above 1 km, we do not see features which are characteristic of stress-induced cracks. A typical mosaic for samples from above 1 km is shown in Figure 5-7. There are a few cracks present, but they are not parallel nor do they cross grain boundaries. Rather, the cracks present in Figure 5-7 are coincident grain boundary cracks which are not characteristic of stress-induced cracks. Many of these cracks also contain healing features.

Through microscopic observations we can also determine the fracture history of this granite core. For example, in

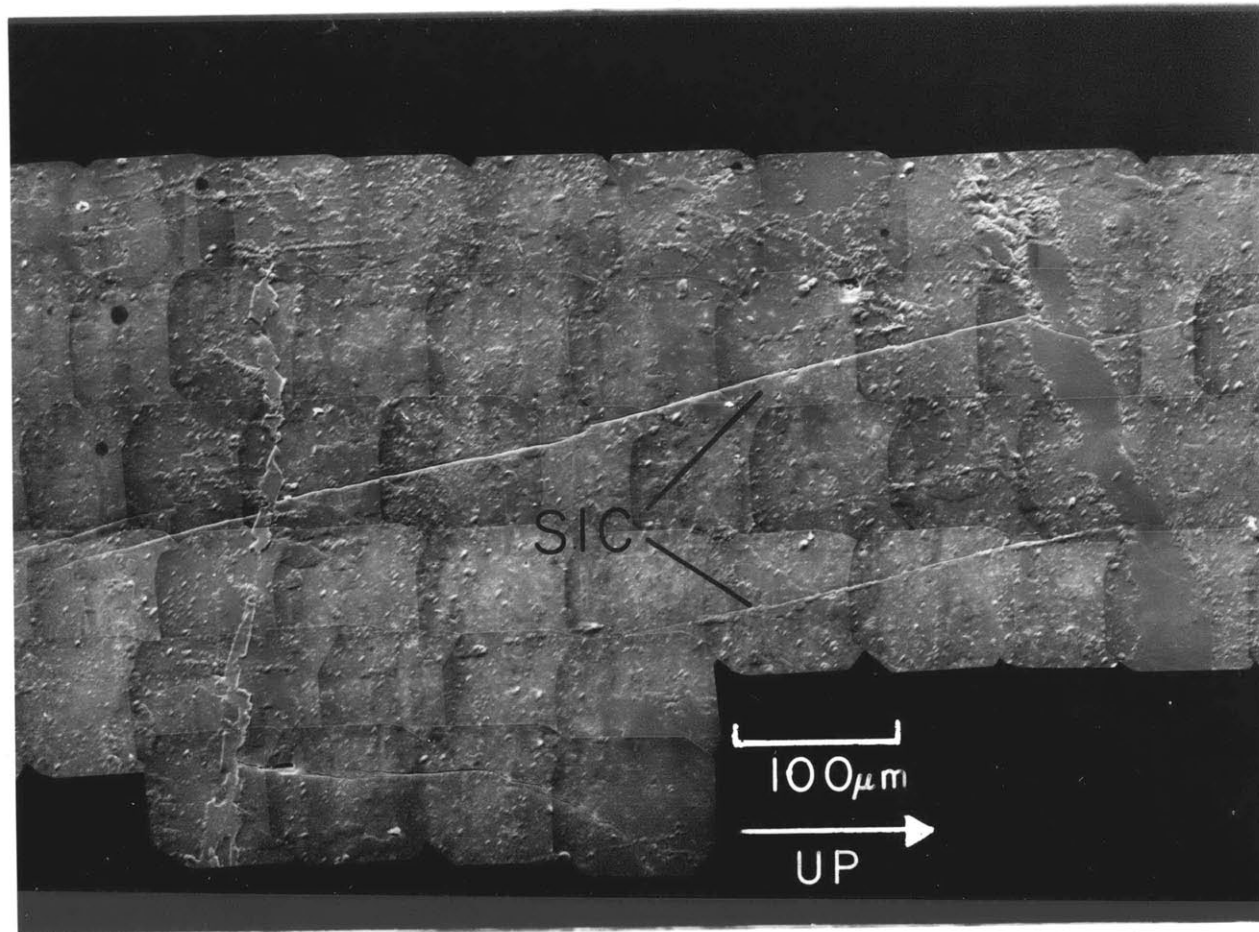


Figure 5-5. Typical texture of Sh-13-1523. The cracks in this SEM micrograph show all the characteristics of SIC. They are transgranular, cross grain boundaries and form parallel sets. The unrounded linear areas are quartz sealed cracks, all other material is microperthite. The orientation of the core axis is indicated by the arrow.

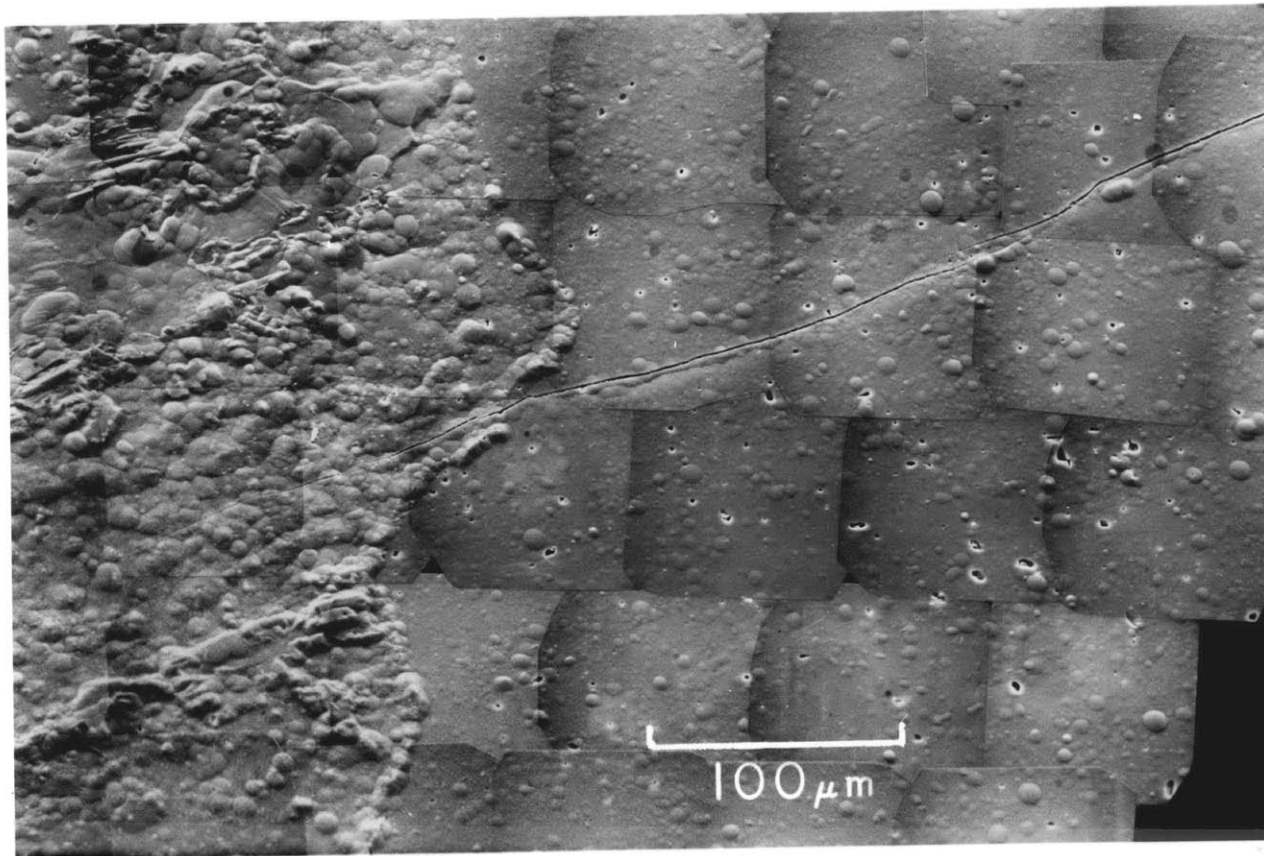
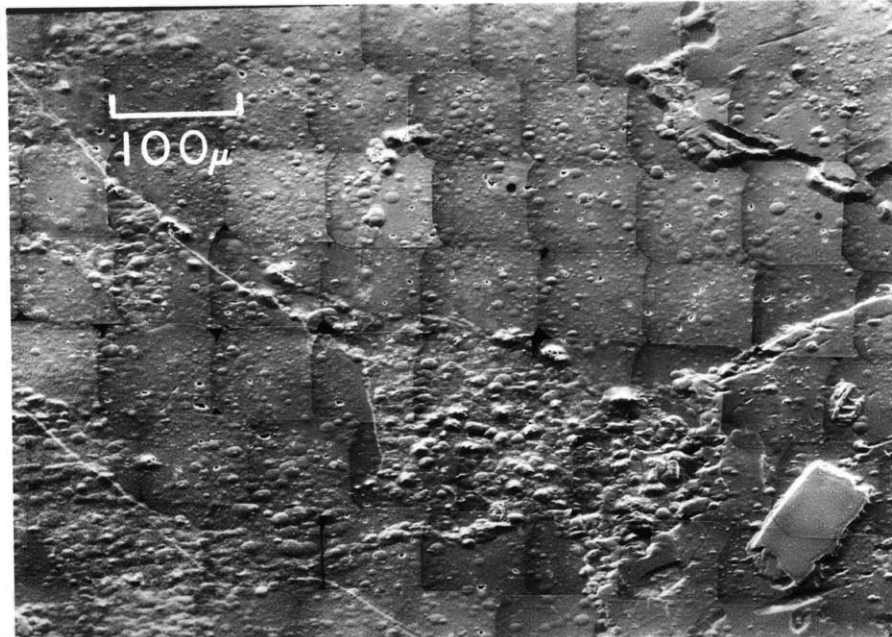
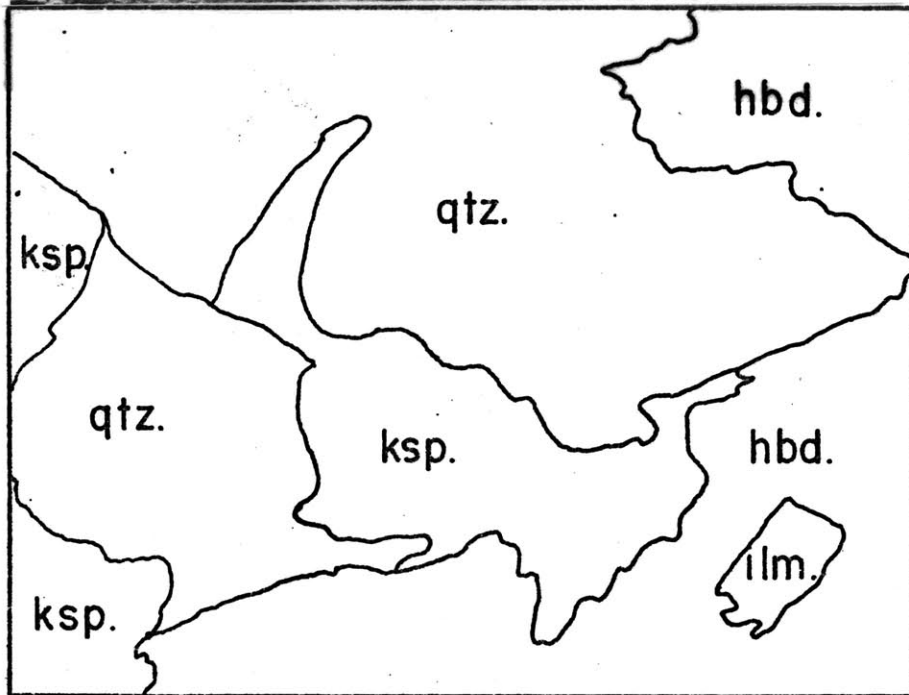


Figure 5-6. Transgranular SIC in Sh-13-1056. This crack crosses the quartz-feldspar grain boundary with no change in orientation. The axis of the core is normal to the plane of the section. SEM micrograph.



5-7a



5-7b

Figure 5-7. Typical texture in Sh-13 samples from above 1 km. Transgranular SIC are not present. The few cracks that are present are partially healed coincident grain boundary cracks. (5-7a) SEM micrograph. (5-7b) Mineral grain map.

Figure 5-8, we see evidence for at least three separate fracturing events. The first fracturing event opened a set of parallel cracks with horizontal orientation. These cracks are now sealed with quartz and are labeled F1. After sealing, fractures (labeled F2) developed in the quartz. These cracks are now partially healed and are marked by planes of fluid inclusions. The third and final fracturing event is indicated by cracks F3. These cracks cross both F1 and F2. Note that cracks F3 are parallel to each other, and by our previous arguments are tectonically stress induced. The set of parallel sealed cracks (F1) may also have been stress-induced. Through examination of healed and sealed cracks such as these, it may be possible to determine both the present and paleo-stress state of rocks.

### Discussion

Observations with the SEM, PM and DSA consistently show the presence of SIC below 1 km in the granite core from Shannon County, Missouri. Results from DSA indicate that many of these SIC have closure pressure of about 150 bars and are oriented vertically, but these 150 bar closure pressure SIC were not present in situ. We propose that they were formed as a result of tectonic stress relief when the core was drilled. The microscopic observations support this conclusion since the observed SIC contain no evidence of healing and were recently formed.



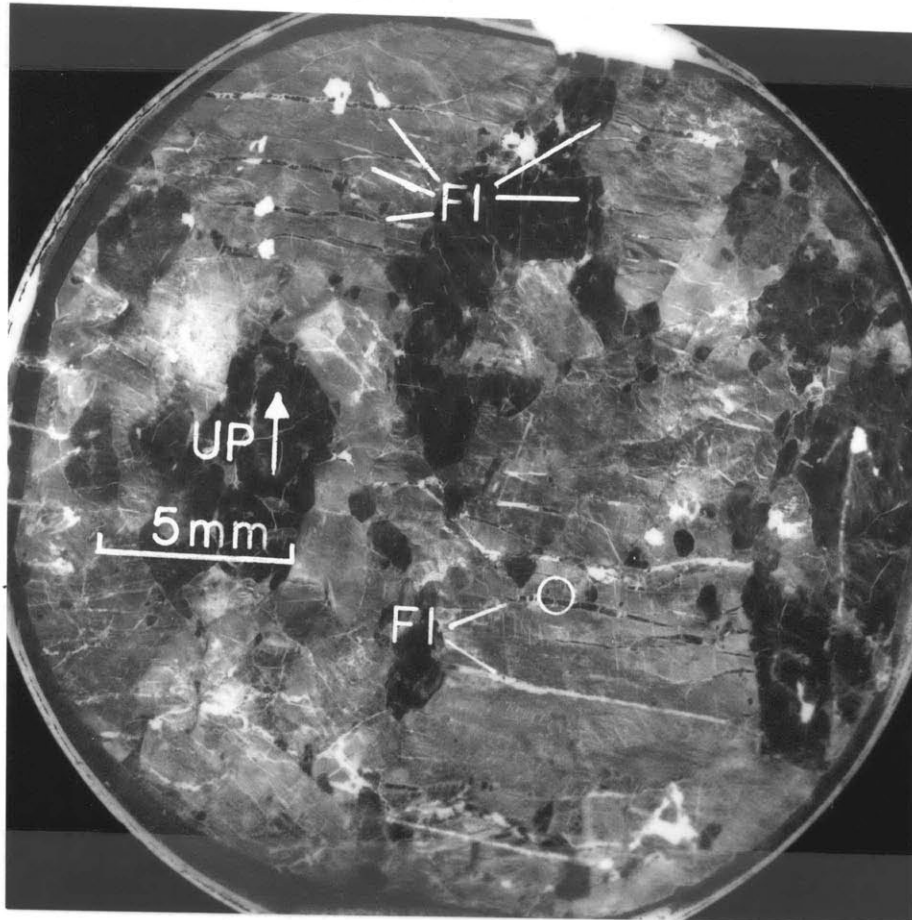
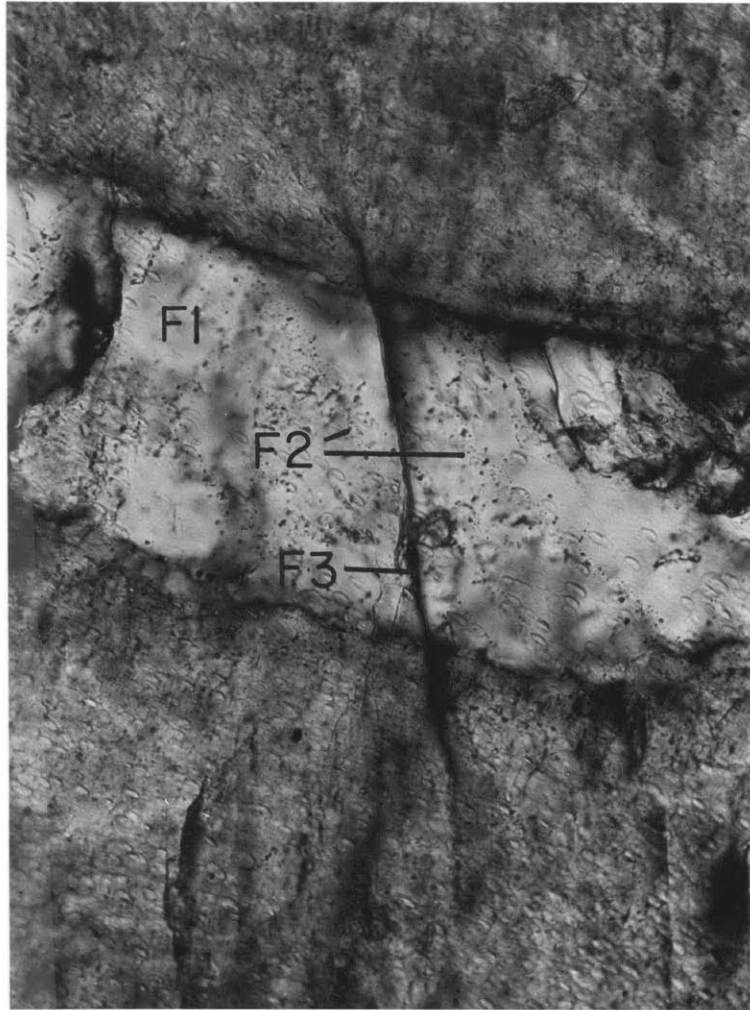


Figure 5-8a. Fracturing episodes in Sh-13-1523. Parallel fractures, F1, formed first and were sealed with quartz. The second fracturing event produced fractures which are now marked by fluid inclusion planes, F2. Both F1 and F2 are cross-cut by the recently formed SIC, F3. See Figure 5-8b for F2 and F3. Negative print, transmitted light.



100  $\mu\text{m}$

Figure 5-8b. Fluid inclusion planes (F2) in quartz sealed crack (F1) which are cross-cut by newly formed SIC (F3). See circled area in Figure 5-8a. Photomicrograph, plane polarized light.

Many workers have examined the relationship between microcracks, joints and in situ stress (Harper, 1966; Norman, 1970; Price, 1959; Wise, 1964). Norman (1970) examined the microcracks in granitic core from Stone Mountain, Georgia, and found that the plane of most microcracks were oriented perpendicular to the direction of maximum compression as determined by borehole deformation gages (Hooker and Duvall, 1966). Norman (1970) also attributed crack formation to stress relief when the core was drilled. Since these stress relief cracks are produced in tension, the magnitude of the maximum in situ compressive stress must be greater than the tensile strength of the rock.

Applying Norman's results to our data, we conclude that the direction of maximum compression is horizontal below 1 km in the vicinity of the Sh-13 borehole. This result is consistent with the results of Sykes and Sbar (1973) and Sbar and Sykes (1973) who used focal mechanisms, in situ overcoring and hydrofracture measurements to determine that the maximum compressive stress is horizontal over large intraplate regions. We cannot as yet determine the azimuthal orientation of the core; nor can we determine the magnitude of the stress because we do not yet know the relationship between crack characteristics and stress magnitude. Examination of cracks produced under triaxial compression or tensile extension may shed light on the value of the stress magnitude.

In Figure 5-8, the SIC formed by stress relief, F3, may

be due to the same stress which produced the parallel sealed cracks, Fl. Consider the following sequence of events: Application of compressive stress produces SIC parallel to the direction of maximum compression. These SIC become sealed with quartz and the locking stresses are balanced by the locked-in stresses (Friedman, 1972). Upon excavation of the core, the stresses are relieved and cracks are produced normal to the direction of maximum compression. The final result is two orthogonal sets of cracks as seen in Figure 5-8.

In conclusion, analysis of cracks in core samples promises to be a useful technique for extending our knowledge of in situ stress states to virtually any depth in boreholes. Present borehole deformation techniques are limited to depths less than 30 meters. Hydrofracture techniques are not depth limited, but they do not yield azimuthal information. We have extended our examination of recently formed SIC to analysis of healed and sealed cracks in core samples. Healed and sealed cracks record the fracture history of rocks and may provide insight into paleostress states and paleotectonics.

## CHAPTER 6

## SUMMARY

Microcracks in rocks produced by uniaxial stress in the laboratory are characterized using SEM and PM observations and measurements of strain to high precision as a function of hydrostatic pressure. Many of our results corroborate the findings of many other workers who observe that stressing produces cracks which are intragranular or transgranular, they may cross several grain boundaries with no change in orientation, and they form parallel to subparallel sets which are parallel to the direction of maximum stress. In addition, we find that many SIC are associated with pre-existing cracks, pre-existing cracks enhance the production of SIC, the closure pressure of many SIC is less than 200 bars and dilatancy is not totally recoverable under zero confining pressure.

The observation that dilatancy is not totally recoverable and pre-existing cracks enhance the production of SIC means that rocks in tectonically active zones will become progressively weaker unless the rate of strain accumulation is slow enough to allow crack healing after an earthquake. The observation that SIC often form parallel sets implies that the physical properties of rocks under stress will be anisotropic. Any program designed to monitor phenomena precursory to earthquakes must consider that observed variations

in measured physical properties may be due to spatial as well as temporal effects.

We have applied our characterization of laboratory SIC to examination of the cracks in a 1.5 km core from southeastern Missouri. Our analysis shows that most SIC are oriented vertically and were produced as a result of tectonic stress relief when the core was drilled. Based upon crack characteristics, we conclude that the maximum stress in the vicinity of this borehole is horizontal. Analysis of cracks in core samples promises to be a useful tool for determining in situ stress states.

Our data from hydrostatically pressure cycled rocks indicates that many cracks do not reopen after the pressure is removed. Therefore, laboratory experiments done under simulated in situ pressure conditions may not be valid analogues. Even if in situ pressure and temperature conditions are duplicated exactly in the laboratory, the crack structure of the rock may not be duplicated exactly, and the interpretation of physical properties measurements will be erroneous. We suggest that physical properties are often best determined from crack characteristics rather than by direct measurements.

## APPENDIX I

## Sh-13 Core Description.

The Sh-13 core was drilled in 1969 and was described by E. Kisvarsanyi. The core is catalogued in Kisvarsanyi (1975).

Depth (feet)	Description
1333	Contact with white, good Lamotte ss. Top 10' is weathered, coarse, reddish granite.
1358	Aplite vein. Granite is slightly porphyritic.
1391-1400	Aplite vein.
1421	Aplite vein (1'). Granite is fairly uniformly medium to coarse grained, often with a porphyritic aspect. Mafics up to 20%, sometimes schlieren-like. Short sections are fractured and slickensided. Effects of weathering manifested by altered mafics and kaolinized feldspars in places, down to about 1490', but it is not the type of porous weathering that is evident at top.
1659	Aplite vein (1').
1760-1767	Very fine grained aplitic dike, has somewhat more mafics than other aplites above (see spl. Sh-13-1765). Also Sh-13-1762 which has a thin seam or lens of coarser grained granite, bleached, in the aplite.
1770-1777	Lighter colored and coarser grained aplite vein. More like a leucogranite.
1777-1810	From here the granite is paler colored, like the leucogranite above. One nearly vertical, 1/2 inch wide basic dike cuts through it.



Depth (feet)	Description
1809-1812	Basic dike in fragmented pieces within granite.
1812-1815	Quartz veins in granite.
1816	Coarse grained granite, as above.
1880-1920	Gradual coarsening of granite.
1918	1/2 foot mixed dike or schlieren, fine grained, dark and light material mixed.
1971	Strikingly porphyritic (spl) granite with large feldspars and coarse clusters of mafics.
2000	The above section gradually changed to a less color contrasted but very similar section. Feldspar composition has probably changed.
2016	Mafic schlieren up to one foot thick, darker color, coarse grained.
2018-2022	
2137	Epidote vein.
2152-2163	Basic dike, dipping 70-80 degrees, sharp contacts.
2171	One foot of fracturing, filled with mafics.
2201	Basic stringer.
2209-2210 1/2	Basic dike.
2285	One foot aplite vein.
2394	1/2 foot aplite vein.
2411	Finer grained, more mafic section, 1 foot.

Depth (feet)	Description
2422-2446	Variable section with mafic and felsic portions.
2446	Variable section continues on down. Light colored portions are highly quartzose.
2476	Basic dike with epidote.
2535-2538	Aplite dike.
2574-2576	Finer grained, mafic dike, mixed.
2581-2595	Aplite variable grain (?).
2604 and below	Mafic content increases.
2626-2631	Several steeply dipping, narrow, mafic dikes.
2677	One foot mixed mafic vein.
2745	Contact of transitional section, one foot, then diorite.
2762	Lower contact of diorite.
2769	Contact of host granite, transitional above.
2745-2769	Variable rock with darker colored dioritic rock in the middle, bordered by transitional sections like spl. Sh-13-2764 below.
2976	Rock type shows slight changes.
2992-2998	Basic dike, gentle dip, sharp contact.
3017-3019	Diorite dike.
3023	1/2 foot diorite dike.
3055	One foot highly fractured section.
3119-3123	Hybrid section.

Depth (feet)	Description
3130	Aplite, 1 foot.
3149	1/2 foot aplite.
3214	Xenolith. Gray color that has been predominant for some time now is becoming gradually pinkish.
3323-3328	Aplite. Fractures filled with dark secondary minerals.
3340-3341	Dark dike, coarse-grained.
3360	Section contains several large (1") xenoliths. Also fracturing.
3451-3452	Altered dike rock.
3501	Aplite, one foot.
3551-3559	Aplite.
3579	Aplite, 2 feet. Many xenoliths, large porphyroblastic feldspars, does not look like a normal granite, more like a hybrid rock.
3598-3618	Dioritic section begins again. Jointed, fractured, color gets gray. Gradational contact from 3616.
3620-3633	Gradually becomes pink, goes back to the coarse, porphyritic granite.
3633-3671	Great aplite dike. Above the transitional contact is due to the aplite's influence on the gray granite or diorite.

Depth (feet)	Description
3638-3640	Basic dike in the aplite.
3749	1/2 foot of coarse lens without sharp contact.
3849-3872	Upper contact of basic dike. Chilled contact, dense, black.
3853	Grades into medium crystalline diabase with good ophitic texture.
3872	Lower contact of diabase dike. Below the dike 1/2 inch wide arsenopyrite (?) vein.
3961-3970	Basic dike, chilled contact, separation of 1 foot aplite in the middle.
3992	Leucogranitic variation without sharp contact.
4003	Very red sample.
4036	Grain size smaller.
4258	3 feet aplite with sharp contact. Granite below is more normal looking.
4328-4353	Aplite, coarser grained towards bottom.
4418	Aplite.
4439-4451	Basic dike.
4474	Quartz druse with hematite in granite.
4489-4544	Fine grained rock with sharp lower contact.
4588	Tiny aplite with gradational contact.
4658	Aplite, 2 feet.
4688-4700	Undulouose contacts of highly quartzose aplite.
4708	Contact with very coarse, quartzose rock, pegmatitic.

Depth (feet)	Description
4730	Dark dioritic material gradually comes in.
4738	Goes back to the pegmatite.
4782-4785	Basic dike.
4799	Leucogranitic, pegmatitic. Very coarse grained, light colored, pinkish. Down to bottom very coarse, good granite.
4989	Schlieren.
5000	Contact with aplite. Bottom of the hole is in aplite.
5004	Bottom.

## REFERENCES

- Anna, J. and G. W. Stose, Geology of Carroll and Frederick Counties, in The Physical Features of Carroll County and Frederick County, Maryland Dept. of Geol., Mines, and Water Resources, 11-128, 1946.
- Aggarwal, Y. P., L. R. Sykes, J. Armbruster, and M. L. Sbar, Premonitory changes in seismic velocities and prediction of earthquakes, Nature, 241, 101-104, 1973.
- Berry, A. W., Jr. and M. E. Bickford, Precambrian volcanics associated with the Taum Sauk caldera, St. Francois Mountains, Missouri, U.S.A., Bull. Volcanol., 36, 308-318, 1972.
- Bickford, M. E. and D. G. Mose, Geochronology of Precambrian rocks in the St. Francois mountains, southeastern Missouri, Geol. Soc. Amer. Spec. Paper 165, 48 pp., 1975.
- Birch, F., The velocity of compressional waves in rocks to 10 kilobars, part 1, J. Geophys. Res., 65, 1083-1102, 1960.
- Birch, F., The velocity of compressional waves in rocks to 10 kilobars, part 2, J. Geophys. Res., 66, 2199-2224, 1961.
- Brace, W. F., Brittle fracture of rocks, in State of Stress in the Earth's Crust, W. R. Judd, editor, American Elsevier Publishing Co., New York, 110-178, 1964.
- Brace, W. F., Some new measurements of linear compressibility of rocks, J. Geophys. Res., 70, 391-398, 1965.

- Brace, W. F., Micromechanics in rock systems, in Structure, Solid Mechanics and Engineering Design, M. Te'eni, editor, Wiley-Interscience, New York, 187-204, 1971.
- Brace, W. F. and E. G. Bombolakis, A note on brittle crack growth in compression, J. Geophys. Res., 68, 3709-3713, 1963.
- Brace, W. F. and A. S. Orange, Electrical resistivity changes in saturated rocks during fracture and frictional sliding, J. Geophys. Res., 73, 1433-1445, 1968.
- Brace, W. F. and A. S. Orange, Further studies of the effects of pressure on electrical resistivity of rocks, J. Geophys. Res., 73, 5407-5420, 1968.
- Brace, W. F., B. W. Paulding, Jr., and C. Scholz, Dilatancy in the fracture of crystalline rocks, J. Geophys. Res., 71, 3939-3953, 1966.
- Brune, J. N., T. L. Henyey, and R. F. Roy, Heat flow, stress, and rate of slip along the San Andreas fault, California, J. Geophys. Res., 74, 3821-3827, 1969.
- Cooper, H.W. and G. Simmons, The effect of cracks on the thermal expansion of rocks, Earth Planet. Sci. Lett., in press, 1977.
- Councill, R. J., The commercial granite of North Carolina, North Carolina Div. of Min. Resources, Bull. No. 67, 59 pp., 1954.
- Cruden, D.M. The static fatigue of brittle rock under uniaxial compression, Int. J. Rock Mech. Min. Sci. & Geomech Abstr., 11, 67-73, 1974.

- Dale, T. N., The commercial granites of New England, U.S. Geol. Surv. Bull. 738, 487 pp., 1923.
- Feves, M. and G. Simmons, Effects of stress on cracks in Westerly granite, Bull. Seism. Soc. Am., 66, 1755-1765, 1976.
- Feves, M., G. Simmons, and R. W. Siegfried, Microcracks in crustal igneous rocks: physical properties, in The Earth's Crust: Its Nature and Physical Properties, J. G. Heacock, editor, Geophys. Monogr. Ser., vol. 20, AGU, Washington, D. C., in press, 1977.
- Filon, N. G., On the elastic equilibrium of circular cylinders under certain practical systems of load, Phil. Trans. R. Soc. London, A198, 147-233, 1902.
- Franklin, J. A., Triaxial strength of rock materials, Rock Mech., 3, 86-98, 1971.
- Friedman, M., R. D. Perkins, and S. J. Green, Observations of brittle deformation features at the maximum stress of Westerly granite and Solenhofen limestone, Int. J. Rock Mech. Min. Sci., 7, 297-306, 1970.
- Friedman, M., Residual elastic strain in rocks, Tectonophysics 15, 297-330, 1972.
- Fuller, M. L., The New Madrid earthquake, U. S. Geol. Surv. Bull. 494, 119 pp., 1912.
- Griffith, A. A., The phenomena of rupture and flow in solids,



- Phil. Trans. R. Soc. London, A221, 163-197, 1921.
- Griffith, A. A., The theory of rupture, Proc. First Int. Cong. Appl. Mech., Delft, 55-63, 1924.
- Gupta, I. N., Premonitory changes in shear velocity anisotropy in Nevada, in Proc. Conf. on Tectonic Problems of the San Andreas Fault System, R. L. Kovach and A. Nur, editors, Stanford University Press, Palo Alto, Calif., 479-488, 1973a.
- Gupta, I. N., Premonitory variations in S-wave velocity anisotropy before earthquakes in Nevada, Science, 182, 1129-1132, 1973b.
- Hadley, K., The effect of cyclic stress on dilatancy: another look, J. Geophys. Res., 81, 2471-2474, 1976.
- Haimson, B. C., Mechanical behavior of rock under cyclic loading, in Advances in Rock Mechanics, Vol. IIA, National Science Foundation, Washington, D. C., 373, 1974.
- Hallbauer, D. K.; H. Wagner, and N. G. W. Cook, Some observations concerning specimens in stiff, triaxial compression tests, Int. J. Rock Mech. Min. Sci. & Geomech. Abstr., 10, 713-726, 1973.
- Hardy, H. R., Jr., Application of acoustic emission techniques to rock mechanics research, in Acoustic Emission, A Symposium, Bal Harbour, Florida, 7-8 December 1971, American Society for Testing and Materials Special Technical Publication 505, Philadelphia, 41 pp., 1972.
- Harper, M. L., Joints and microfractures in Glenwood Canyon,

- Colorado, The Mountain Geol., 3, 185-192, 1966.
- Hast, N., The state of stress in the upper part of the earth's crust, Tectonophysics, 8, 169-211, 1969.
- Henye, T. L. and G. J. Wasserberg, Heat flow near major strike-slip faults in California, J. Geophys. Res., 76, 7924-7946, 1971
- Hooker, V. and W. I. Duvall, Stresses in rock outcrops near Atlanta, GA, U. S. Bur. Mines, Rept. Invest. 6860, 18 pp., 1966.
- Hooker, V. E. and C. F. Johnson, Near-surface horizontal stresses including the effects of rock anisotropy, U. S. Bur. Mines, Rept. Invest. 7224, 29 pp., 1969
- Kisvarsanyi, E. B., Operation basement: buried Precambrian rocks of Missouri - their petrography and structure, Am. Assoc. Petroleum Geologists Bull., 58, 674-684, 1974.
- Kisvarsanyi, E. B., Data on Precambrian in drillholes of Missouri including rock type and surface configuration, Missouri Dept. of Natural Resources, Rept. Invest. 56, 19 pp., 1975.
- Kisvarsanyi, G. and E. B. Kisvarsanyi, Ortho-polygonal tectonic patterns in the exposed and buried Precambrian basement of southeast Missouri, in Proc. First International Conf. on the New Basement Tectonics, R. L. Hodgson, editor, Utah Geological Assn., Salt Lake City, 169-182, 1976.

- Knill, J. L., J. A. Franklin, and A. W. Malone, A study of acoustic emission from stressed rock, Int. J. Rock Mech. Min. Sci., 5, 87-121, 1968.
- Kropotkin, P. N., The state of stress in the earth's crust as based on measurements in mines and on geophysical data, Phys. Earth Planet. Interiors, 6, 214-218, 1972.
- Lachenbruch, A. H. and J. H. Sass, Thermo-mechanical aspects of the San Andreas fault system, in Proc. Conf. on Tectonic Problems of the San Andreas Fault System, R. L. Kovach and A. Nur, editors, Stanford University Press, Palo Alto, Calif., 192-205, 1973.
- Lockwood, R. P., Petrology of syenites, Wausau, Wisconsin, Wisconsin Compass, 48, 32-44, 1970.
- Matsushima, S., Variation of the elastic wave velocity of rocks in the process of deformation and fracture under high pressure, Disaster Prevention Res. Inst. Bull. 32, Kyoto Univ., 1-8, 1960.
- Mjachkin, V. I., W. F. Brace, G. A. Sobolev, and J. H. Dieterich, Two models for earthquake forerunners, PAGEOPH, 113, 169-181, 1975.
- Mogi, K., Study of elastic shock caused by the fracture of heterogeneous materials and its relations to earthquake phenomena, Tokyo University, Bull. Earthquake Res. Inst., 40, 125-173, 1962.
- Mogi, K., Some precise measurements of fracture strength of rocks under uniform compressive stress, Rock Mech. Eng.

- Geol., 4, 41-55, 1966.
- Mogi, K., Source locations of elastic shocks in the fracturing process in rocks (1), Tokyo University Bull. Earthquake Res. Inst., 46, 1103-1125, 1968.
- Morlier, P., Description de l'état de fissuration d'une roche à partir d'essais non-destructifs simples, Rock Mech., 3, 125-138, 1971.
- McClintock, F. A. and J. B. Walsh, Friction on Griffith cracks in rocks under pressure, Proc. Natl. Cong. Appl. Mech., 4th, Berkeley, 1015-1021, 1962.
- Norman, C. E., Geometric relationships between geologic structure and ground stresses near Atlanta, GA, U. S. Bur. Mines, Rept. Invest. 7365, 24 pp., 1970.
- Nur, A., Effects of stress on velocity anisotropy in rocks with cracks, J. Geophys. Res., 76, 2022-2034, 1971
- Nur, A., Dilatancy, pore fluids and premonitory variation of ts/tp travel times, Bull. Seism. Soc. Am., 62, 1217-1222, 1972.
- Nur, A. and G. Simmons, The effect of saturation on velocity in low porosity rocks, Earth Planet. Sci. Lett., 7, 183-193, 1969a.
- Nur, A. and G. Simmons, Stress-induced velocity anisotropy in rock: an experimental study, J. Geophys. Res., 74, 6667-6674, 1969b.
- Nur, A. and G. Simmons, The origin of small cracks in igneous rocks, Int. J. Rock Mech. Min. Sci., 7, 307-314, 1970.

- Obert, L. and W. Duvall, The microseismic method of predicting rock failure in underground mining, U. S. Bur. Mines, Rept. Invest. 3803, 1945.
- Obert, L., S. L. Windes, and W. I. Duvall, Standardized tests for determining the physical properties of mine rock, U. S. Bur. Mines, Rept. Invest. 3891, 1946.
- Paulding, B. W., Jr., Crack growth during brittle fracture in compression, PhD thesis, Massachusetts Institute of Technology, 1965.
- Peng, S. and A. M. Johnson, Crack growth and faulting in cylindrical specimens of Chelmsford granite, Int. J. Rock Mech. Min. Sci., 9, 37-86, 1972.
- Peselnick, L., R. Meister, and W. H. Wilson, Pressure derivatives of elastic moduli of fused quartz to 10 kb, J. Phys. Chem. Solids, 28, 635-639, 1967.
- Price, N. J., Mechanics of jointing in rocks, Geol. Mag., 96, 149-167, 1959.
- Quinn, A., Settling of heavy minerals in a granodiorite dike at Bradford, Rhode Island, Amer. Min., 28, 272-281, 1943.
- Richter, D. and G. Simmons, Thermal expansion behavior of igneous rocks, Int. J. Rock Mech. Min. Sci. & Geomech. Abstr., 11, 403-411, 1974.
- Richter, D. and G. Simmons, Microcracks in crustal igneous rocks: microscopy, in The Earth's Crust: Its Nature and Physical Properties, J. G. Heacock, editor, Geophys.

- Monogr. Ser., vol. 20, AGU, Washington, D. C., in press, 1977a.
- Richter, D. and G. Simmons, Microscopic tubes in igneous rocks, Earth Planet. Sci. Lett., 34, 1-12, 1977b.
- Robertson, E. C., Experimental study of the strength of rocks, Bull. Geol. Soc. Am., 66, 1275-1314, 1955.
- Sbar, M. L. and L. R. Sykes, Contemporary compressive stress and seismicity in eastern North America: an example of intraplate tectonics, Bull. Geol. Soc. Am., 84, 1861-1882, 1973.
- Schock, R. N. and H. C. Heard, Static mechanical properties and shock loading response of granite, J. Geophys. Res., 79, 1662-1666, 1974.
- Scholz, C. H., Microfracturing of rock in compression, PhD thesis, Massachusetts Institute of Technology, 1967.
- Scholz, C. H., Microfracturing and the inelastic deformation of rock in compression, J. Geophys. Res., 73, 1417-1432, 1968.
- Scholz, C. H., Post-earthquake dilatancy recovery, Geology, 2, 551-554, 1974.
- Scholz, C. H. and R. Kranz, Notes on dilatancy recovery, J. Geophys. Res., 79, 2132-2135, 1974.
- Scholz, C. H., L. R. Sykes, and Y. P. Aggarwal, Earthquake prediction, a physical basis, Science, 181, 803-810, 1973.
- Semenov, A. M., Variation in the travel-time of transverse and longitudinal waves before violent earthquakes,

- Izv. Earth Phys., no. 4, 72-77, 1969, Engl. trans. in Physics of the Solid Earth, no. 1, AGU, 245-248, 1969.
- Siegfried, R. W., Differential strain analysis: application to shock induced microfractures, PhD thesis, Massachusetts Institute of Technology, 1977.
- Siegfried, R. W. and G. Simmons; Characterization of oriented cracks with differential strain analysis, J. Geophys. Res., accepted, 1977.
- Simmons, G., Velocity of shear waves in rocks to 10 kilobars, part 1, J. Geophys. Res., 69, 1123-1130, 1964.
- Simmons, G. and H. W. Cooper, Thermal cycling cracks in three igneous rocks, Int. J. Rock Mech. Min. Sci. & Geomech. Abstr., submitted, 1977.
- Simmons, G. and D. Richter, Microcracks in rocks, in The Physics and Chemistry of Minerals and Rocks, Proc. of NATO Petrophysics Meeting, April 1974, R. G. J. Strens, editor, Wiley-Interscience, New York, 105-137, 1976.
- Simmons, G., R. W. Siegfried, and M. Feves, Differential strain analysis: a new method for examining cracks in rocks, J. Geophys. Res., 79, 4383-4385, 1974.
- Simmons, G., R. Siegfried, and D. Richter, Characteristics of microcracks in lunar samples, Proc. Lunar Sci. Conf. 6th, 3, 3227-3254, 1975.
- Skehan, J. W., Symp. on Quarrying in Massachusetts, in Economic Geology in Massachusetts, O. C. Farquhar, editor, 1967.

- Sprunt, E. S. and W. F. Brace, Direct observation of micro-cavities in crystalline rocks, Int. J. Rock Mech. Min. Sci., 11, 139-150, 1974.
- Stuckey, J. L. and S. G. Conrad, Explanatory text for geologic map of North Carolina, North Carolina Div. of Min. Resources, Bull. No. 71, 51 pp., 1958.
- Sykes, L. R. and M. L. Sbar, Intraplate earthquakes, lithospheric stresses and the driving mechanism of plate tectonics, Nature, 245, 298-302, 1973.
- Tabet, D. E., Structure and petrology of the Mellen igneous intrusive complex near Mellen, Wisconsin, University of Wisconsin, Masters thesis, 81 pp., 1974.
- Tapponier, P. and W. F. Brace, Development of stress-induced microcracks in Westerly granite, Int. J. Rock Mech. Min. Sci. & Geomech. Abstr., 13, 103-112, 1976.
- Todd, T. P., Effect of cracks on elastic properties of low porosity rocks, PhD thesis, Massachusetts Institute of Technology, 328 pp., 1973.
- Todd, T., D. A. Richter, G. Simmons, and H. Wang, Unique characterization of lunar samples by physical properties, Proc. Lunar Sci. Conf. 4th, 3, 2639-2662, 1977a.
- Todd, T., G. Simmons, and W. S. Baldrige, Acoustic double refraction in low-porosity rocks, Bull. Seism. Soc. Am., 63, 2007-2020, 1973b.
- Tolman, C. F. and F. Robertson, Exposed Precambrian rocks in southeast Missouri, Missouri Geol. Survey and Water



- Resources, Rept. Invest. 44, 68 pp., 1969.
- Tuttle, O. F., Structural petrology of planes of liquid inclusions, J. Geol., 57, 331-356, 1949.
- Walsh, J. B., The effect of cracks on the compressibility of rock, J. Geophys. Res., 70, 381-389, 1965.
- Walton, W. H., Mechanical Properties of Non-Metallic Brittle Materials, Interscience, New York, 491 pp., 1958.
- Wawersik, W. R. and W. F. Brace, Post-failure behavior of a granite and diabase, Rock Mech., 3, 61-85, 1971.
- Wawersik, W. R. and C. Fairhurst, A study of brittle rock failure in laboratory compression experiments, Int. J. Rock Mech. Min. Sci., 7, 561-575, 1970.
- Whitcomb, J. H., J. D. Germany, and D. L. Anderson, Earthquake prediction: variation of seismic velocities before the San Fernando earthquake, Science, 180, 632-635, 1973.
- Winkler, E. M., Stone: Properties, Durability in Man's Environment, Springer-Verlag, New York, 230 pp., 1973.
- Wise, D. U., Microjointing in basement, middle rocky mountains of Montana and Wyoming, Geol. Soc. Am. Bull., 75, 287-306, 1964.
- Zoback, M. D. and J. D. Byerlee, The effect of cyclic differential stress on dilatancy in Westerly granite under uniaxial and triaxial conditions, J. Geophys. Res., 80, 1526-1530, 1975a.
- Zoback, M. D. and J. D. Byerlee, The effect of microcrack dilatancy on the permeability of Westerly granite,

J. Geophys. Res., 80, 752-755, 1975b.

## BIOGRAPHICAL NOTE

The author was born in Portland, Oregon and graduated from U.S. Grant High School in June 1969. Undergraduate education was obtained at Reed College, The University of Washington, and Portland State University. A B.A. degree in physics from Reed College was received in May 1973 and the author was voted: Commendation for Excellence in Scholarship by the faculty of Reed College. Graduate work at MIT was supported by teaching and research assistantships (research funded by the Office of Naval Research contract N00014-76-C-0478).

At the time of writing the author is 26 years of age. He is happily married to the former Gloria Carolyn Lohman and has a 2 year old daughter, Jordana Lohman.

## Publications:

Feves, M. and G. Simmons, Effects of stress-induced cracks and saturation on  $V_p$ , (abst), Eos, Trans. AGU, 55, 433, 1974.

Simmons, G., R. W. Siegfried, and M. Feves, Differential strain analysis: a new method for examining cracks in rocks, J. Geophys. Res., 79, 4383, 1974.

Feves, M. and G. Simmons, Stress-induced cracks in Westerly granite, (abst), Eos, Trans. AGU, 56, 447, 1975.

Simmons, G., D. Richter, R. W. Siegfried, and M. Feves, Microcracks in ancient rocks, (abst), Eos, Trans. AGU, 57, 327, 1976.

- Feves, M. and G. Simmons, Effects of stress on cracks in Westerly granite, Bull. Seismo. Soc. Am., 66, 1755, 1976.
- Feves, M., G. Simmons, and R. W. Siegfried, Microcracks in crustal igneous rocks: physical properties, in The Earth's Crust: Its Nature and Physical Properties, Geophys. Monogr. Ser., vol. 20, edited by J. G. Heacock, AGU, Washington, D. C., in press, 1977.
- Feves, M. and G. Simmons, The relationship of microcracks to in situ stress in southeastern Missouri, (abst), Geol. Soc. Am., 8, 864, 1976.
- Feves, M. and G. Simmons, The relationship of pre-existing cracks to stress-induced cracks in rocks, (abst), Eos, Trans. AGU, 58, 500, 1977.